Dominance reversal protects large-effect resistance polymorphisms in temporally varying environments

Marianthi Karageorgi[1,7], Anastasia S. Lyulina[1,2], Mark C. Bitter[1], Egor Lappo[1], Sharon I. Greenblum[3], Zach K. Mouza[1], Caitlynn T. Tran[1], Andy V. Huynh[1], Hayes Oken[4], Paul Schmidt[4,6,7], and Dmitri A. Petrov[1,5,6,7]

1. Department of Biology, Stanford University, Stanford, CA 94305, USA
2. Department of Applied Physics, Stanford University, Stanford, CA 94305, USA
3. Department of Energy Joint Genome Institute, Lawrence Berkeley National Laboratory, Berkeley, CA 94720, USA
4. Department of Biology, University of Pennsylvania, Philadelphia, PA 19104, USA
5. CZ Biohub, San Francisco, CA 94158
6. These authors contributed equally
7. Corresponding authors: M.K. (mkarag@stanford.edu), P.S. (schmidtp@upenn.edu), and D.A.P (dpetrov@stanford.edu)

Abstract

A central challenge in evolutionary biology is to uncover mechanisms maintaining functional genetic variation in heterogeneous environments[1,2]. Population genetics theory suggests that beneficial reversal of dominance, where alleles are dominant when beneficial and recessive when deleterious, can help maintain such variation in temporally varying environments[3,4]. However, empirical examples are scarce[5] due to difficulties in measuring dominance in fitness in field experiments[6]. Here we quantify the selective effects and dominance of large-effect insecticide-resistant alleles at the *Ace* enzymatic locus in *Drosophila melanogaster*[7]. In laboratory assays, we identify a beneficial reversal of dominance of the *Ace* alleles for fitness-associated phenotypes under selection in the presence and absence of malathion, a widely used organophosphate insecticide. Using highly replicated field mesocosms, we show that resistant *Ace* alleles fluctuate rapidly in response to a pulse of malathion, but are maintained in its absence. We show that this pattern is only consistent with beneficial reversal of dominance, where the resistant *Ace* alleles are dominant and beneficial for resistance and recessive and deleterious for enzymatic function. Moreover, we find that seasonally fluctuating selection due to insecticide resistance can generate fluctuating chromosome-scale genomic perturbations of allele frequencies. We propose an extension to Wright's physiological theory of dominance[8], arguing that under fluctuating selection the currently deleterious allele should often behave as loss-of-function and thus recessive to the currently beneficial allele. Overall, our results suggest that beneficial reversals of dominance can be common and can help both maintain genetic variation and allow for rapid evolutionary responses to environmental shifts.

42 **Main text**

43 The maintenance of functional additive genetic variation for fitness-related traits in
44 populations, and specifically the portion that is due to the segregation of large-effect loci, has
45 long posed a theoretical and empirical challenge[9,10]. Classical population genetics theory
46 suggests that directional selection should erode such variation over time. However, the observed
47 persistence of intermediate-frequency large-effect loci in natural populations implies that
48 balancing selection mechanisms, including spatial or temporal environmental variation in
49 selection pressures, may be a prevalent force acting on natural populations[11].

50 As one example, studies of seasonal dynamics in Drosophila revealed the presence of
51 large-effect seasonal polymorphisms[12,13] that rapidly respond to environmental fluctuations, with
52 the causal alleles shifting between advantageous to deleterious multiple times during a single
53 seasonal cycle[14–16]. Some of these seasonal alleles have strong enough selective effects that they
54 can change frequencies by tens of a percent per season, yet still remain polymorphic over
55 hundreds of thousands or even millions of generations[12].

56 One mechanism proposed by theoretical models that can strongly stabilize genetic
57 variation in the face of temporal fluctuations is beneficial reversal of dominance[3,4,17]. This
58 phenomenon occurs when each allele is partially or completely dominant in environments in
59 which it is favored and recessive in environments in which it is harmful. Such reversals of
60 dominance act as a stabilizing mechanism by protecting recessive deleterious alleles from
61 selection and precluding their loss. At the same time, it allows a rapid response to selection
62 shifts, as adaptive alleles are always dominant, even when rare. Even modest beneficial reversal
63 of dominance has been shown to help preserve variation under fluctuating selection in single- or
64 multiple-locus models and to allow fluctuating selection to drive allele frequency fluctuations[4].

65 The central empirical questions are twofold: does beneficial reversal of dominance occur
66 for functional polymorphic large-effect loci across the genome, and does it naturally arise within
67 genetic systems? The overall scarcity of empirical examples[5] makes these questions difficult to
68 answer, as measuring fitness and the dominance of fitness effects in natural environments
69 remains a challenge[6].

70 To begin addressing this knowledge gap, here we investigate the dominance of large-
71 effect alleles conferring resistance to organophosphate insecticides at the *Ace* locus in natural
72 populations of *Drosophila melanogaster*. *Ace* encodes acetylcholinesterase (AChE), a key
73 enzyme in the insect nervous system responsible for breaking down acetylcholine[18].
74 Organophosphate insecticides, introduced in the 1950s and 1960s, act as irreversible inhibitors of
75 AChE, causing insect death by binding to its active site and preventing removal of acetylcholine
76 from the synapses upon firing[19]. These insecticides have imposed seasonally fluctuating selection
77 pressures on *D. melanogaster* populations, as seen in seasonal resistance fluctuations in field
78 studies[20,21]. This case is a compelling example of a large-effect polymorphism subject to
79 fluctuating selection, where the causal locus, the mechanistic basis of selection, and the
80 conditions that confer advantage to alternative alleles are well understood. Here we first analyze
81 genomic data from worldwide *D. melanogaster* populations to assess whether patterns of
82 resistant *Ace* allele frequencies are consistent with spatially and temporally variable insecticide
83 use. We then combine laboratory and outdoor mesocosm experiments to measure fitness effects
84 and dominance in the presence and absence of organophosphates, serving as proxies of the two
85 alternative environments.

86 Previous studies have identified several resistant *Ace* alleles in natural *D. melanogaster*
87 populations carrying resistance mutations at four conserved sites near the AChE active site

88 (I161V, G265A, F330Y, G368A), with those carrying the VGFG and VAYG resistance
89 haplotypes as the most common[7,22] (**Fig. 1a**). Our analysis of two inbred line panels, LNPA[14] and
90 DGRP[23], collected from a farmers market in Pennsylvania and an orchard in North Carolina,
91 respectively, confirmed these two as the most common resistant *Ace* alleles. Further, the LNPA
92 population also carries another resistance haplotype VGFA at frequency ~13% (**Fig. 1a,**
93 **Extended Data Fig. 1**). Using the Drosophila Evolution Over Space and Time (DEST) dataset,
94 which sampled *D. melanogaster* populations worldwide across seasons and years[24], we tracked
95 the I161V mutation shared by all three resistant *Ace* alleles as a marker for resistance.
96 The I161V polymorphism displayed seasonal fluctuations of up to 33% per season (**Fig.**
97 **1b**) and its frequency varied from 1 to 85 % (**Fig. 1c**) in the 34 cases where we had paired
98 Spring and Fall samples from the same year at the same location in natural populations. The
99 variation of the frequency across all sampled populations in the Spring was more extreme
100 compared to the empirical null defined by studying matched control SNPs (ECDF test, p=
101 0.0018) (**Fig. 1d**). These findings support our notion that seasonally varying organophosphate
102 selection induces strong and rapidly fluctuating selection at the *Ace* locus.

Figure 1

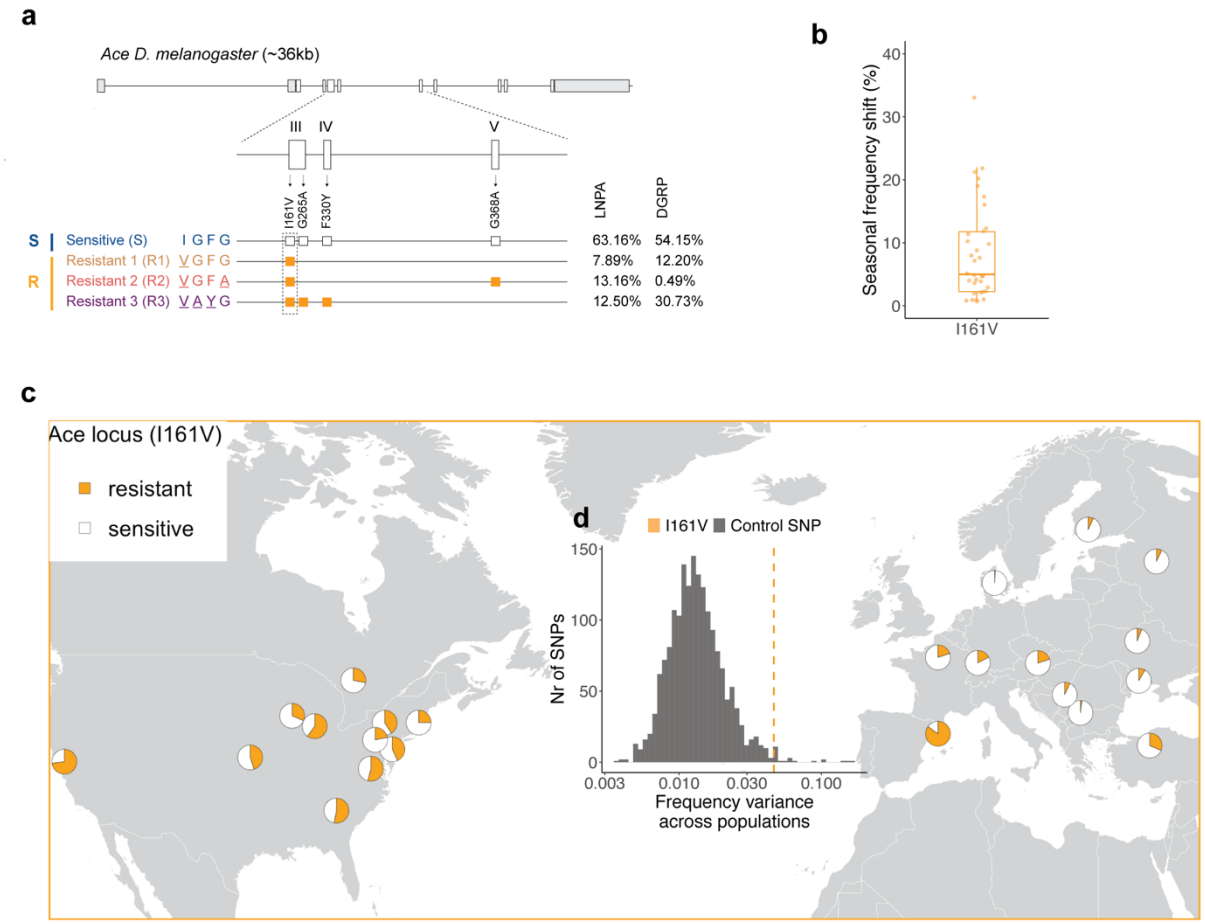

103

Figure 1. Organophosphate-resistant *Ace* alleles display seasonal fluctuations and are present at intermediate frequencies in natural *Drosophila melanogaster* populations. a, Four widespread organophosphate resistance target site mutations in the *Ace* gene coding for acetylcholinesterase (AChE) in *D. melanogaster*. Frequencies of sensitive (S: IGFG) and common resistant *Ace* alleles with three different resistance haplotypes (R1: VGFG, R2: VGFA, R3: VAYG) in DGRP and LNPA panels of fully sequenced inbred lines (See also **Extended Data Figure 1**). **b-d,** Temporal and spatial dynamics of the shared organophosphate resistance polymorphism I161V present in common resistant *Ace* alleles in worldwide populations (data from the DEST database, see also **Methods**). Absolute allele frequency shift of I161V from Spring to Fall across populations (points for individual populations) (**b**), allele frequency map of I161V (**c**), and comparison of the variance of frequency of I161V (dashed orange line) to matched control SNPs across populations (log scale, ECDF test of SNP frequency variances, p = 0.0118) (**d**).

We next used a laboratory-based approach to assess the dominance of resistant *Ace* alleles over their sensitive counterparts for fitness-associated phenotypes likely to be under selection in organophosphate-rich and -free environments. The resistance mutations confer a resistance benefit in the presence of insecticides by altering the shape of AChE's active site, thus preventing insecticide binding[7]. However, these same mutations impair AChE activity and stability[25], likely rendering them deleterious in the absence of insecticides[26].

Using the LNPA panel of inbred lines, which contains the sensitive and three resistant *Ace* alleles (**Fig. 1a**, **Extended Data Fig. 1**), we generated recombinant populations with homozygous sensitive, homozygous resistant, and heterozygous genotypes for each resistant allele (S: IGFG, R1: VGFG, R2: VGFA, R3: VAYG) (see **Methods**). This approach[27] allowed us to control for the genotype at the *Ace* locus while allowing variation in the rest of the genome. This enabled us to measure effects specifically due to the *Ace* genotypes while reducing the influence of unlinked genetic variation.

We first estimated resistance to organophosphates using malathion LD_{50} values (dose causing 50% egg-to-adult mortality). For resistance conferred by insensitivity to malathion, the level of dominance *h* of resistant alleles is measured by the ratio (LD_{50}[RS] - LD_{50}[SS])/(LD_{50}[RR]-LD_{50}[SS]). The resistant R2 and R3 *Ace* alleles significantly increased malathion LD_{50} by ~5.8x and ~7.8x respectively ($p < 0.001$ for both), and were highly dominant over the sensitive S *Ace* allele, with dominance *h* 0.78 and 0.77 for R2 and R3, respectively ($p < 0.001$ for both). In contrast, the R1 *Ace* allele showed no significant increase in malathion resistance ($p = 0.646$) and no clear dominance pattern ($h = -1.29$, $p = 0.751$) (**Fig. 2, Extended Data Fig. 2, Extended Data Table 1**). The dominance of resistance is expected because malathion covalently binds to and inactivates the sensitive S *Ace* allele, while the resistant alleles

127 remain functional. This pattern follows Wright's physiological theory of dominance[8], which
128 predicts that functional alleles are dominant over loss-of-function alleles, as even one copy of the
129 functional allele provides sufficient enzyme activity.

130 We next assessed the cost of resistance in the absence of organophosphates by
131 quantifying two key fitness-associated phenotypes, viability (egg to adult survival) and fecundity
132 (number of eggs laid by gravid females). All homozygous resistant genotypes exhibited lower
133 phenotypic fitness values compared to the homozygous sensitive genotype, for either or both of
134 these phenotypes, with viability reductions ranging from 12.4% to 16.9% (all $p < 0.001$) and
135 fecundity reductions from 16.2% (R2R2, $p = 0.37$) to 46.8% (R3R3, $p < 0.001$). The costs driven
136 by the three resistant alleles were either significantly recessive for at least one of the phenotypes
137 (viability R2: $h = 0.17$, $p = 0.027$, fecundity R3: $h = -0.02$, $p = 0.001$), or indistinguishable from
138 codominance (**Fig. 2g-l, Extended Data Tables 2-3**). Overall, the sensitive S *Ace* allele is
139 beneficial and dominant/codominant and never recessive towards its resistant counterparts in
140 terms of viability and fecundity in the absence of malathion.

141 These results are consistent with the beneficial reversal of dominance. They also suggest
142 that the response to organophosphates at the concentrations similar to the LD_{50} of the sensitive
143 homozygous genotype should induce a very rapid increase in the frequency of the resistant *Ace*
144 alleles and in the level of overall resistance, given that resistant *Ace* alleles are strongly
145 beneficial and dominant. We also expect that in the absence of insecticides, the resistant *Ace*
146 alleles should only show slow declines in frequency when rare given that they are recessive.
147 However, if previous insecticide exposure has caused these alleles to become common in the
148 population, their subsequent decline (when insecticides are removed) should occur much more
149 rapidly.

Figure 2

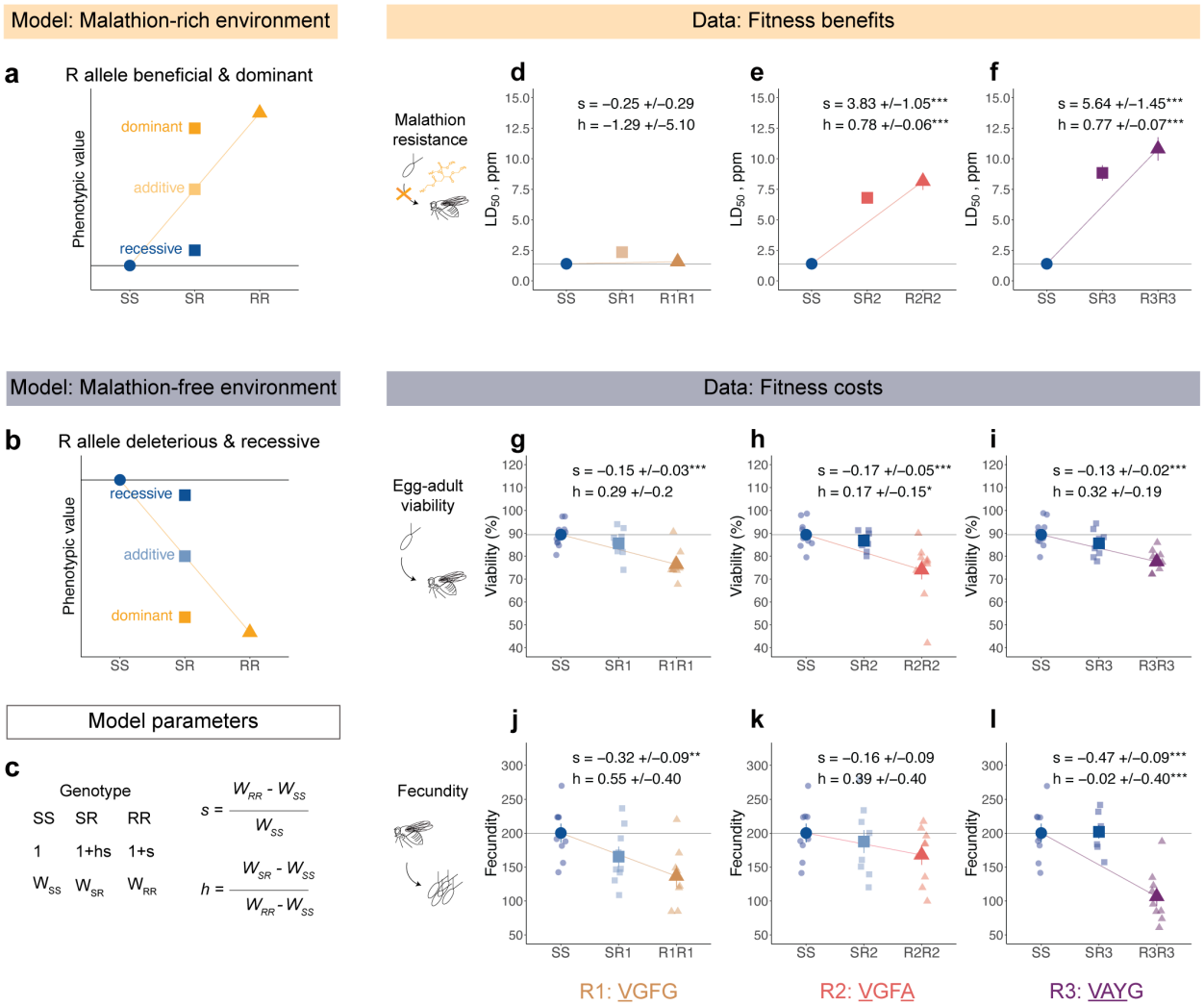

150

Figure 2. Beneficial reversal of dominance of organophosphate-resistant *Ace* alleles for fitness-associated phenotypes relevant to malathion-rich and -free environments. a-b, In a scenario of a beneficial reversal of dominance, the resistant R *Ace* alleles are beneficial and partially or completely dominant in malathion-rich environments, but deleterious and recessive in malathion-free environments. **c,** Selection (*s*) and dominance (*h*) coefficients for each fitness-associated phenotype are estimated based on the viability selection model. **d-l,** Comparison of malathion LD_{50} (**d, e, f**), egg-adult viability (n= 10 technical replicates, 50 eggs/replicate) (**g, h, i**), and fecundity (n= 8-10 technical replicates, 5 females/bottle/3 days) (**j, k , l**) among *Ace* genotypes. For calculation of malathion LD_{50} see **Methods** and **Extended Data Figure 2**. Egg-adult viability and fecundity data were analyzed with logistic and linear regression models. Points represent the mean ± s.e.m for each *Ace* genotype. Bootstrapping analysis was performed to assess whether the selection and dominance coefficients significantly differ from 0 and 0.5, respectively. The asterisks indicate significant differences (* <0.05, **< 0.01, ***<0.001). The color of the heterozygote for each *Ace* allele corresponds to its dominance based on the beneficial reversal of dominance model. Statistical tests in **Extended Data Table 1-3**.

151 To test these predictions, we directly investigated the population dynamics at the *Ace*
152 locus in an ecologically realistic environment by evolving replicate *Drosophila melanogaster*
153 populations in the presence and absence of seasonally fluctuating malathion in field mesocosms
154 at an experimental orchard in Pennsylvania (**Fig. 3a,** see **Methods**). We established 20 replicate
155 populations derived from a baseline population constructed from the LNPA panel of 76 inbred
156 lines used in our lab experiments (**Extended Data Figure 1**). These lines were outbred for 4
157 generations in large indoor cages before ~1000 males and females were used to seed each
158 outdoor cage (see **Methods** and Bitter and colleagues[28]). The initial frequencies of the resistant
159 *Ace* alleles in the field mesocosms likely reflect their frequencies in the local population from
160 which the LNPA lines were derived.

161 After the first ~4 weeks (3-4 generations) of untreated propagation, the 20 outdoor cages
162 were divided into ten malathion-treated and ten untreated cages. To mimic natural insecticide
163 exposure, we applied gradually increasing concentrations of commercial malathion (Southern Ag
164 Malathion 50% E.C.) in the growth media of the treated populations, 1.5-2.5 ppm from July 21
165 to August 24, 2021, followed by 7.5 ppm until September 6, 2021. These doses, based on our lab
166 LD_{50} measurements, exert strong selection against different *Ace* alleles, with lower doses
167 targeting the S and R1 alleles, and higher doses affecting the R2 and R3 alleles (**Extended Data**
168 **Fig. 2**). Following the malathion exposure, the experiment continued without pesticides in all 20
169 cages through December 22, 2021. Throughout the experiment, we tracked population dynamics,
170 malathion resistance, and genome-wide allele frequencies at eight timepoints (~every one to two
171 generations), focusing on trajectories of resistant *Ace* alleles and linked sites in response to
172 fluctuating malathion exposure (**Fig. 3a**).

Figure 3

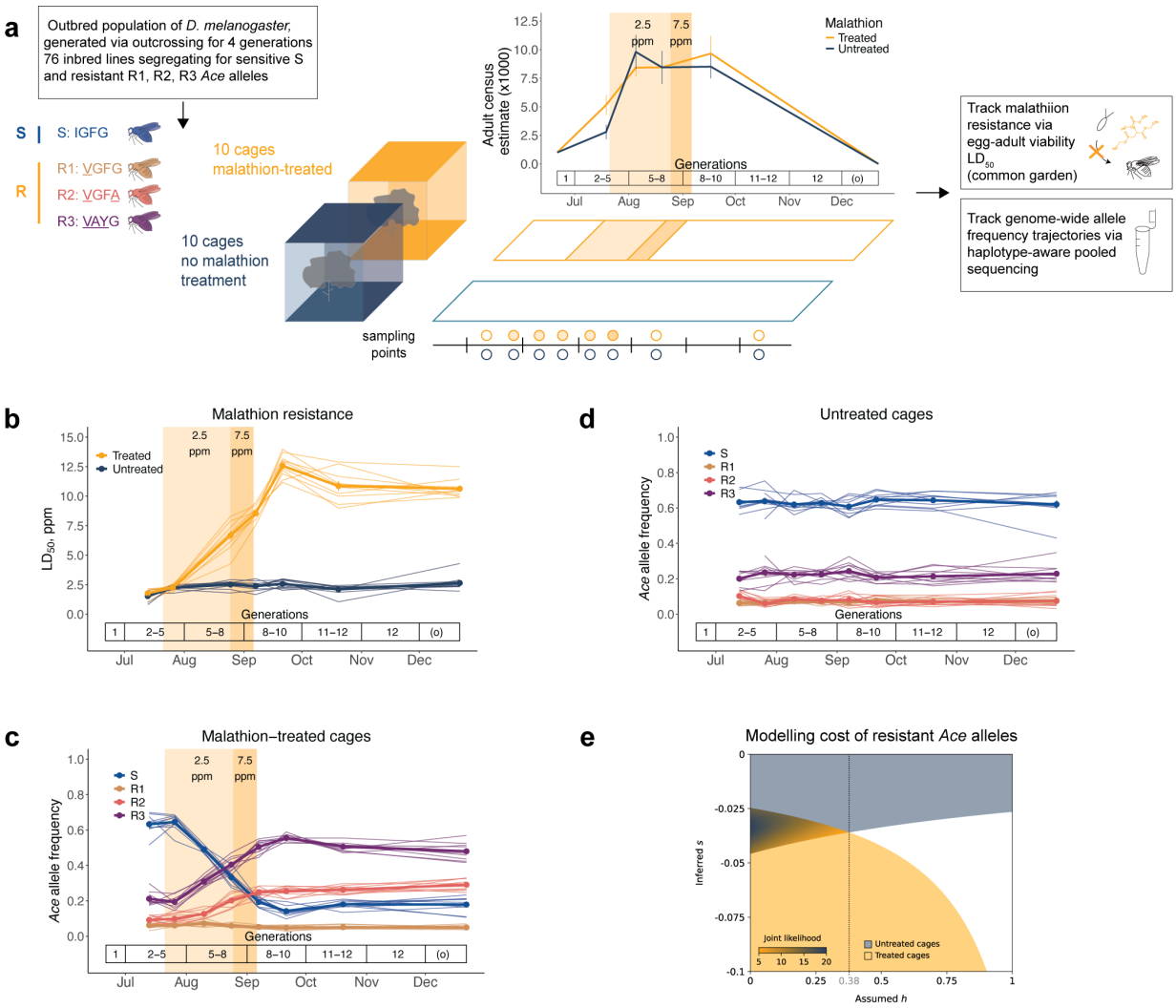

173

Figure 3. Beneficial reversal of dominance of resistant *Ace* alleles for fitness in an ecologically realistic environment. a, Twenty field mesocosm cages were seeded with an outbred population of *D. melanogaster* generated via outcrossing for 4 generations 76 inbred lines carrying the sensitive S and resistant R1, R2, and R3 Ace alleles. Ten cages received a malathion pulse after the initial population establishment. Eight timepoints were sampled to track the evolution of malathion resistance and genome-wide allele in the treated and untreated populations. Malathion did not affect estimated adult fly population sizes (mean ± s.e.m.) in treated populations. **b,** The malathion pulse led to a significant increase and subsequent decline of resistance (LD_{50}, ppm) in the treated populations while resistance remained stable in the untreated populations. For LD_{50} calculations see **Methods** and **Extended Data Figure 3**. Light lines/points show individual populations (orange, treated; blue, untreated), dark lines/points represent mean ± s.e.m. (n=10 populations per treatment group). **c-d,** Trajectories of *Ace* alleles in treated (**c**) and untreated (**d**) populations. In treated populations, the malathion pulse led to a significant increase in the frequency of the resistant R2 and R3 *Ace* alleles, followed by a decline in the frequency of R3. *Ace* allele frequencies remained stable in the untreated populations. Light lines/points show individual allele trajectories, dark lines/points represent the mean ± s.e.m. (n = 10 populations per treatment group). (**continued on next page**)

Figure 3 (continued). e, Inferred selection (s) and dominance (h) coefficients from changes in the resistant *Ace* allele frequency. The colored ranges show the selection coefficients corresponding to the 0.95 confidence intervals of the slope distribution, obtained by bootstrapping cages within each treatment group. The overlap between the orange (treated cages) and dark blue (untreated cages) restricts the possible values of *s* and *h*. Within that overlap, lower values of *h* better explain both sets of data, as shown by higher values of the joint likelihood calculated from the bootstrap distributions (see **Methods**). All results of statistical tests can be found in **Extended Data Tables 4-6**.

Surprisingly, the seasonal population dynamics were qualitatively similar in both malathion-treated and untreated cages (**Fig. 3a**). In all cages, population sizes increased through the summer months until reaching maximum size and then slowly declined in late Fall as abiotic conditions worsened. We interpret the unchanged seasonal population dynamics as an indication that population dynamics in all cages are primarily determined by high levels of baseline egg, larval, and pupal mortality that mask additional mortality imposed by malathion on the adult census population.

To characterize malathion resistance, we tracked egg to adult survival on diets with 0-15 ppm malathion and estimated LD_{50} at each timepoint per population (see **Methods** and **Extended Data Fig. 3**). In malathion-treated cages, resistance increased rapidly from ~2.2 ppm to ~12.6 ppm during exposure ($t = 24.26$, $p < 0.001$), followed by a significant decline to ~10.6 ppm after removal of malathion ($t = -3.96$, $p = 0.001$) (**Fig. 3b, Extended Data Table 4.1**). In contrast, resistance levels in untreated cages remained stable at ~2.2 ppm throughout the experiment ($t = 1.07$, $p = 0.288$) (**Fig. 3b, Extended Data Table 4.2**).

Using a haplotype-aware method to analyze pooled sequencing data[29], we inferred the frequency dynamics of the sensitive and resistant *Ace* alleles (see **Methods**). In treated cages, resistant *Ace* alleles R2 and R3 increased significantly during malathion exposure (R2: $t = 13.93$, $p < 0.001$; R3: $t = 27.59$, $p < 0.001$), with R3 subsequently declining post-exposure ($t = -5.18$, $p < 0.001$) (**Fig. 3c, Extended Data Table 5**). The R1 allele showed muted responses, consistent

193 with our lab data showing that it confers no detectable malathion resistance (**Fig. 2c, Extended**
194 **Data Table 5**). In untreated populations, all resistant *Ace* allele frequencies remained stable (all
195 $p > 0.05$) (**Fig. 3d, Extended Data Table 6**).

196 To assess the contribution of the resistant *Ace* alleles to malathion resistance evolution in
197 the field mesocosms, we applied a viability selection model using lab-measured *Ace* genotype
198 viabilities (see **Methods**). This model closely recapitulated both the allele frequency trajectories
199 (**Extended Data Fig. 4a,b**) and the evolution of malathion resistance (**Extended Data Fig. 4c,d**)
200 observed in the field mesocosms. The agreement between model predictions and experimental
201 data provides compelling evidence that *Ace* was the major effect locus conferring malathion
202 resistance in the treated cages.

203 The results from the field mesocosms were qualitatively consistent with our expectations.
204 The *Ace* genetic system exhibited two key behaviors, rapid response to malathion exposure and
205 maintenance of resistance at low levels in its absence. In the malathion-treated cages, we
206 observed a significant decline of high-frequency resistant *Ace* alleles post malathion exposure,
207 indicating considerable fitness costs for resistant alleles when common. In contrast, untreated
208 cages showed fairly stable frequencies of low-frequency resistant alleles, suggesting low
209 selection coefficients (s) or dominance parameters (h) in the absence of malathion.

210 To obtain bounds on evolutionary parameters, we fit the allele frequency data of the
211 treated and untreated cages to a viability selection model where all resistant alleles share the
212 same fitness cost (see **Methods**). The model that fits both datasets best had low cost ($s \sim 2.5$ to
213 5%) and low dominance values ($h < 0.38$) (**Fig. 3e, Extended Data Fig. 5**). At higher values of
214 h, there is no single selection coefficient that can explain the patterns of allele frequency change
215 for both treated and untreated cages, and the likelihood of the data is higher the closer h is to

216 zero. Overall, the data are consistent with the fitness cost of organophosphate resistance being
217 recessive and low, allowing the resistant *Ace* alleles to persist at low frequencies for extended
218 periods of time.

219 The rapid frequency fluctuations of large-effect alleles are expected to generate long-
220 range allele frequency perturbations. However, in most situations these effects are difficult to
221 quantify as the patterns of linkage of common large-effect variants are complex. Our system
222 presents a rare opportunity to do this as we have the information of starting haplotypes and thus
223 at least the starting patterns of linkage of SNPs genome-wide with the Ace alleles. Using a two-
224 step approach (see **Methods** for details), we first employed quasibinomial logistic regression to
225 estimate allele frequency changes (effect sizes) for genome-wide SNPs during malathion
226 exposure (July 26 to September 21, 2022) and post-exposure (September 21 to December 22,
227 2021). Second, we identified the SNPs tightly linked (Ace-linked) and loosely linked (control) to
228 the sweeping R2 and R3 *Ace* alleles across the genome, based on patterns of linkage in our
229 inbred lines. This approach allowed us to quantify the extent of both the forward *Ace* sweep
230 during malathion exposure and the reverse *Ace* sweep post-exposure.

231 During the malathion exposure, we observed a large selective sweep (~4-10 Mbp) on the
232 3R chromosome arm driven by the *Ace* resistant alleles in the malathion-treated populations. The
233 effect sizes of linked variation were consistently elevated above the control baseline (**Fig. 4a**).
234 Additionally, peaks on arms 2R and 3L were elevated equally for both Ace-linked and control
235 sites, suggesting the presence of two additional resistance loci (**Fig. 4a**). In untreated
236 populations, the frequencies of the R2 and R3 *Ace* alleles remained stable (**Fig. 3c**). As expected,
237 Ace-linked sites in untreated populations did not show any changes in frequency (**Fig. 4b**).

Figure 4

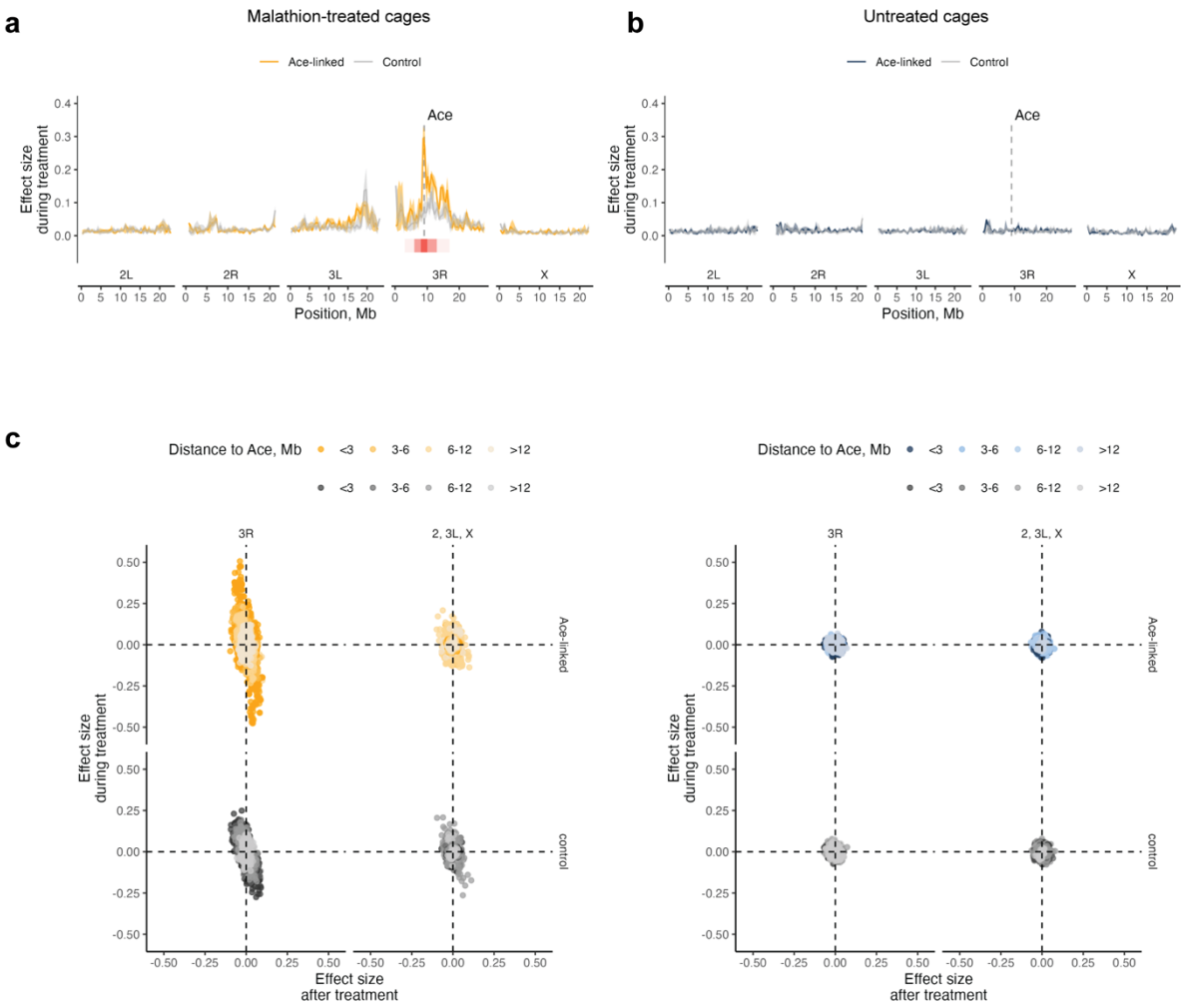

Figure 4. Strong fluctuating selection of resistant *Ace* alleles caused chromosome-scale forward and reverse sweeps during and after malathion treatment, respectively. a-b, Median allele frequency change (effect size) estimated via quasibinomial logistic regression modeling for Ace-linked and unlinked control SNPs in 500kb windows across the genome in malathion-treated (**a**) and untreated (**b**) populations during malathion treatment. The shaded areas represent 95% bootstrap confidence intervals. Sweep width was estimated with bootstrap and is represented with red rectangles on panel a (dark red, middle red, and light red rectangles correspond to 2.5%, 50%, and 97.5% bootstrap quantiles for sweep width, respectively. **c-d,** Comparison of effect size for Ace-linked (top) and unlinked control (bottom) SNPs during (y-axis) and after malathion treatment (x-axis) in malathion-treated (**c**) and untreated populations (**d**). SNPs on chromosomal arm 3R (left) while SNPs on chromosomes 2, X, and the 3L arm (right). Ace-linked and unlinked control SNPs are color-coded by distance from *Ace* locus(dark to light orange, malathion-treated; dark to light blue: untreated).

240 After the malathion exposure, we observed a reverse sweep driven by the *Ace* resistant
241 alleles in the malathion-treated populations. Ace-linked SNPs on the 3R chromosome showed a
242 negative association between frequency changes during and after malathion exposure, with
243 stronger reversals closer to the *Ace* locus compared to less-linked control SNPs (**Fig. 4c,** left top
244 and bottom). We did not observe significant patterns of reversal for either Ace-linked or control
245 SNPs on other chromosomes with treatment (**Fig. 4c,** right top and bottom) or in untreated
246 populations (**Fig. 4d)**. Overall, our analysis confirmed that strong fluctuating selection on
247 resistant *Ace* alleles caused long-range, almost chromosome-scale allele frequency perturbations.
248 Here we provide compelling laboratory evidence for beneficial reversal of dominance at a
249 locus subject to strong, temporally fluctuating selection. Based on these measurements we
250 predicted the rapid increase in frequency of the resistant *Ace* alleles in the presence of
251 organophosphates and the relative stability in their absence. A large-scale highly replicated field
252 mesocosm experiment confirmed our predictions and revealed genome-wide fluctuating sweeps
253 driven by the resistant *Ace* allele. A viability-selection model suggests that the cost of resistance
254 is likely recessive, as only a recessive cost is consistent with the observed stability when rare and
255 the reduction in frequency when common.
256 These results allow us to speculate as to the likely mechanistic reasons for the dominance
257 reversals in fitness we observe. Consistently with previous studies, resistance is beneficial in the
258 presence of organophosphates[7] and costly in its absence[25]. We reasoned that in the presence of
259 organophosphates the benefit should be dominant because loss of function in one copy of the
260 protein will be compensated by the sufficient function of the resistant copy. This follows
261 Wright's physiological theory of dominance[8] that argues that reduction in enzymatic activity by
262 one half should have only a small effect on fitness. Similarly, in the absence of

263 organophosphates the cost should be recessive since the sensitive allele maintains normal
264 function and the logic of the physiological model of dominance applies again.

265 This beneficial reversal of dominance extends Wright's model of dominance as the
266 identity of the dominant beneficial allele changes with the environment. This model also
267 suggests that beneficial reversal of dominance may be a general feature of balanced allelic
268 arrangements where alternative alleles lose their functional capacities across environments due to
269 tradeoffs. One can easily imagine that such scenarios are common and generic and do not require
270 special fine-tuning between fitness and dominance. For example, loci involved in resistance to
271 synthetic insecticides and host plant toxins, which are under temporally varying selection, likely
272 exhibit similar dominance patterns[30,31].

273 An important implication of beneficial reversal of dominance is the capacity to help
274 maintain very large-effect polymorphism and allow for rapid evolutionary responses to
275 environmental change. As we observed in our experiment, fluctuating selection acting on such
276 loci will result in large-scale perturbations of allele frequencies at the causal loci as well as at
277 linked loci at long genomic scales. These perturbations would be hard to detect without knowing
278 the exact linkage structure[32], because the signatures left in the genomic sequences are complex
279 and are unlike what one expects with selective sweeps by *de novo* mutation. However, if the
280 genome contains even a modest number of large effect allele displaying dominance reversal in
281 response to fluctuating selection this by itself can maintain genome-wide functional
282 polymorphisms on long time-scales.

283 To conclude, our work demonstrates that beneficial reversal of dominance operates at
284 least at some loci of large fitness effect, facilitating both rapid responses to shifting selection
285 pressures and the long-term maintenance of polymorphism. We present arguments for why such

reversals should arise commonly and naturally as a simple consequence of the less active (nearly loss-of-function) alleles being recessive as suggested by Wright's theory of dominance. We also introduce a way to quantify dominance in fitness by measuring allele trajectories under selection starting at different frequencies. This approach can be used to assess the presence of beneficial reversal of dominance for loci of large effect segregating in populations across a range of taxa.

Acknowledgements This project was supported by grants from the National Institute of General Medical Sciences of the National Institutes of Health (Award number 1K99GM143455-01 to M.K, Grant 5R01GM100366-08 and 5R01GM137430-02 to P.S., Award Number 5R35GM118165-07 to D.A.P), the CZ Biohub (to D.A.P.), the Sarah Hotchkis Ketterer Graduate Fellowship from Stanford University (to A.S.L.), the National Science Foundation (Grant PRFB 2109407 to M.C.B.), and the Stanford Biology Summer Undergraduate Research Program (to Z.K.M. and A.H.). The authors thank Marcus Feldman for helpful discussions and assistance with modeling *Ace* allele frequency evolution, Danae Papadopetraki for assistance with statistical analyses of the phenotypic and genomic data, Axel Wiberg for feedback on statistical analyses of the genomic data, Emily Behrman for feedback on the day degree model for generation estimation, Jessica Rhodes for helpful discussions and assistance with statistical analyses of the DEST data, and Anastasia Andreeva for assistance with phenotyping. The authors acknowledge Jean Villa for feedback that improved the earlier versions of the manuscript.

Author Contributions M.K was responsible for conceptualization, formal analysis, investigation, writing original draft, writing-review and editing, and visualization; A.L. was responsible for formal analysis, visualization, and writing-review and editing; M.B. was responsible for formal analysis and investigation; E.L. was responsible for formal analysis and visualization; S.G. was responsible for formal analysis; A.H., CT, and Z.K.M. were responsible for investigation; P.S. and D.A.P. jointly supervised the research. P.S. was responsible for conceptualization, investigation, writing-review and editing, and funding acquisition. D.A.P. was responsible for conceptualization, formal analysis, writing-review and editing, and funding acquisition.

314 **Methods**

315

316 **Population genomic analysis for variation of organophosphate-resistant *Ace* alleles over**

317 **space and time**

318 We first conducted a literature review to compile all known naturally segregating target site

319 resistance mutations in the acetylcholinesterase (*Ace* gene) protein of *D. melanogaster* that

320 confer resistance to organophosphates. Mutero and colleagues in 1994[33] first identified the

321 resistance mutations F115S, I199V, I199T, G303A and F368Y, and numbered them based on the

322 precursor acetylcholinesterase (AChE) protein. Menozzi and colleagues in 2004[7] identified

323 combinations of the resistance mutations I161(199)V, G265(303)A, F330(368)Y and

324 G368(406)A in worldwide organophosphate-resistant *D. melanogaster* strains and numbered

325 them based on the mature AChE protein (numbers in the brackets refer to the precursor AChE

326 protein). They did not identify the resistance mutation F77(115)S. At position 77, the mutation

327 TTC to T**C**C changes phenylalanine to serine (Chr3R: 9,070,101, v5.39). At position 161, the

328 mutation ATC to **G**TC changes the isoleucine to valine (Chr3R:9,069,721, v5.39). At position

329 265, the mutation GGC to G**C**C changes the glycine to alanine (Chr3R:9,069,408 , v5.39). At

330 position 330, the mutation TTT to T**A**T changes the phenylalanine to tyrosine (Chr3R:9,069,054

331 , v5.39). At position 368, the mutation GGC to G**C**C/G**CT** changes the glycine to alanine

332 (Chr3R: 9,063,921 , v5.39). The AChE protein's numbering changed between the studies after its

333 crystallization in 2000, which defined the N-terminal signal peptide and the C-terminal

334 sequence[34]. The mutation G368A was misannotated in the study on adaptation of *D.*

335 *melanogaster* to organophosphate insecticides by Karasov and colleagues[22].

336

337 <u>Organophosphate-resistant *Ace* alleles in DGRP and LNPA inbred lines</u>

338 We characterized the presence of organophosphate-resistant *Ace* alleles in two fully
339 sequenced inbred line panels, the Drosophila Genetic Reference Panel (DGRP) and our LNPA
340 panel of inbred lines. The DGRP panel consists of 205 inbred lines derived from wild-caught
341 females collected at the Raleigh, North Carolina Farmers Market in 2003[23]. The LNPA panel
342 consists of 76 inbred lines derived from wild-caught individuals collected in Spring and Fall
343 from Linvilla Orchards, Media PA USA[14]. Both panels contain the two common resistant *Ace*
344 alleles (Ace-R1: VGFG and Ace-R3: VAYG) at high frequency, the sensitive *Ace* allele (Ace-S:
345 IGFG), and other rare resistant alleles. The LNPA panel also contains the resistant *Ace* allele
346 Ace-R2: VGFA at high frequency. We used the LNPA panel for our lab and field mesocosm
347 experiments.
348
349 Seasonal and spatial variation of organophosphate-resistant *Ace* alleles in natural *Drosophila*
350 *melanogaster* populations
351 We used the DEST (Drosophila Evolution Over Space and Time) database to characterize
352 variation in resistant *Ace* allele frequencies between Spring and Fall and across populations. Our
353 analysis focused on the resistant *Ace* allele coding for I161V, a marker for common resistant
354 alleles, as it is shared among them. We selected paired samples of wild-caught populations from
355 locations with both spring/summer (March-August) and fall/winter (September-December) data
356 within the same year, retaining the earliest Spring/Summer and latest Fall/Winter sample for
357 each location-year combination. Based on these criteria, we ended up with 34 paired samples
358 collected between 2012 and 2016.
359 To analyze temporal variation, we calculated the absolute frequency shift of the I161V
360 allele from Spring to Fall for each population per year. For spatial variation, we calculated I161V

361 average frequency at each population in Spring samples across available years and visualized its
362 spatial distribution in an allele frequency map.
363 To further assess the spatial variability of the resistance polymorphism I161V, we
364 compared the I161V allele variance to matched control single nucleotide polymorphisms (SNPs)
365 in the Spring samples across locations. We selected 1000 matched control SNPs based on the
366 following criteria: (1) located within 2Mb from 100kb away from *Ace* to avoid linked SNPs, (2)
367 within the ln(3R)K cosmopolitan inversion to match inversion status, and (3) average frequency
368 across all Spring samples within 4% of the median frequency of the I161V resistance mutation.
369 Finally, we used the cumulative distribution function (CDF) to quantify how extreme the I161V
370 variance was compared to the control SNPs.
371
372 **Lab experiments to estimate dominance of resistant *Ace* alleles for fitness-associated**
373 **phenotypes in presence and absence of malathion**
374 To assess whether the dominance of each resistant *Ace* allele (Ace-R1: VGFG, Ace-R2: VGFA,
375 Ace-R3: VAYG) over their sensitive counterpart (Ace-S: IGFG) reverses for fitness-associated
376 phenotypes that are primarily under selection in organophosphate-rich and -free environments,
377 we first used our LNPA panel of inbred lines to generate recombinant populations with
378 homozygous sensitive, homozygous resistant, and heterozygous *Ace* genotypes for each *Ace*
379 allele. This step was meant to bring potential deleterious, recessive mutations in the inbred lines
380 into heterozygosity. We then measured malathion resistance, viability and fecundity in
381 homozygous and heterozygous populations for each *Ace* genotype.
382
383 Generation of recombinant populations with homozygous sensitive, homozygous resistant, and
384 heterozygous *Ace* genotypes

385 To generate recombinant populations for each *Ace* allele, we first intercrossed 2-3 inbred
386 lines with the same *Ace* allele using a round robin cross scheme (e.g., Line_1 SS x Line_2 SS,
387 Line_2 SS x Line_3 SS, Line_3 SS x Line_1 SS) to bring all founders with the same *Ace* allele
388 together (10 non-mated females x 10 males per round robin cross). We then combined 16 F1
389 flies (8 non-mated females and 8 males) from each of the round robin crosses per *Ace* allele to
390 establish the next generation. Subsequently, we maintained the homozygous populations in vials
391 and allowed them to recombine for four generations until we performed the phenotype
392 measurements. We used lines 12LN6-70_(B33), 12LN6-92_(B3), LNPA-3 for the sensitive *Ace*
393 allele (Ace-S: IGFG), lines 12LN6-86_(B29) and LNPA-53 for the R1 resistant *Ace* allele (Ace-
394 R1: VGFG), lines LNPA-14, LNPA-17 and LNPA-87 for the R2 resistant *Ace* allele (Ace-R2:
395 VGFA), and lines 12LN6-45_(B26), 12LN6-82_(B4), and 12LN6-94_(B19) for the R3 resistant
396 *Ace* allele (Ace-R3: VAYG).
397
398 Measurements of fitness-associated phenotypes
399 For all experiments, we first set up breeding cages with ~ 500 4-to-7-day-old flies of
400 homozygous or heterozygous populations for the sensitive and the resistant *Ace* alleles. To
401 generate the heterozygous recombinant populations, we crossed SS non-mated females with
402 homozygous males of each resistant allele (R1R1, R2R2, R3R3).
403 To compare the level of malathion resistance among the different alleles, we measured
404 egg-to-adult viability on diets that ranged in malathion concentration from 0 ppm to 30 ppm. For
405 this, we collected eggs of each population that were laid within a period of 24 hours and then
406 introduced 50 eggs of each population into narrow vials containing approximately 7 ml of
407 Drosophila growth media supplemented with the respective malathion concentration. We tested

408 each of the malathion concentrations in duplicate vials. We used commercial malathion of 50%
409 strength (Southern Ag Malathion 50% E.C.) and dissolved it in the Drosophila growth media.
410 This medium was kept overnight at 4ºC and used the next day for the assay. We monitored adult
411 eclosion every evening over a period of 10 days until all adult flies had enclosed.
412 To compare viability among the different genotypes, we introduced 50 eggs of each
413 population into narrow vials containing ~7 ml of Drosophila growth media. Each of the
414 genotypes were tested in 10 replicate vials. We monitored adult eclosion every evening over a
415 period of 7 days until all adult flies had enclosed.
416 To compare fecundity among the different genotypes, we used density-controlled (~50
417 eggs/vial) adult female progeny of each population. We introduced five 3-day-old females of
418 each genotype in egg-laying bottles fitted with egg-laying caps filled with Drosophila growth
419 media. Each day over a period of 3 days we counted the number of eggs laid. Each of the
420 genotypes were tested in 8-10 replicate egg-laying bottles. The egg-laying caps were examined
421 under a stereoscope where we counted the eggs laid each day over the 3-day period.
422
423 Statistical analysis of fitness-associated phenotypes
424 We analyzed fecundity, viability, and malathion resistance for the three genotypes (SS,
425 SR, RR) of each *Ace* allele (R1, R2, R3) using R (version 4.2.2). For fecundity and viability, we
426 fitted linear and logistic regression models, respectively, calculating estimated marginal means
427 and performing pairwise comparisons adjusted for multiple testing using the Benjamini-
428 Hochberg procedure. We then implemented a bootstrap procedure (1,000 resamples) to estimate
429 deviation from additivity, selection coefficient, and dominance coefficient. Deviation from
430 additivity was calculated as W[SR] - (W[SS] + W[RR]) / 2, where W represents fitness

431 (fecundity or viability) for each genotype. The selection coefficient *s* was computed as (W[RR] –
432 W[SS]) / W[SS], indicating the relative fitness of the resistant genotype compared to the
433 sensitive genotype. The dominance coefficient *h* was calculated as (W[SR] – W[SS]) / (W[RR] –
434 W[SS]), measuring the degree to which the heterozygote phenotype is closer to either
435 homozygote. Significance was assessed by testing whether results differed from zero (additivity
436 and selection) or 0.5 (dominance). For malathion resistance, we estimated LD_{50} values for each
437 genotype using four-parameter logistic dose-response models f(x) = c + (d-c) / (1 + e^(b(x-e))),
438 where e is LD_{50}, d (upper limit) = 100%, c (lower limit) = 0%, and b is the relative slope around
439 e. For this, we used the L.4() function in the drc package (version 3.0.1)[35] in R (version 4.2.2)
440 with egg to adult viability at the range of malathion concentrations as the response variable. We
441 then used a bootstrap procedure (1,000 resamples) to compare LD_{50} values between genotypes
442 and calculate the same coefficients, substituting LD_{50} values for W in the formulas. For all
443 analyses, bootstrap resampling was used to calculate confidence intervals and p-values, with
444 significance assessed against null hypotheses of 0 (additivity and selection) and 0.5 (dominance).
445

446 **Field mesocosm experiments to track evolution of malathion resistance and genome-wide**
447 **allele frequencies in the presence and absence of fluctuating malathion selection**

448 Experimental orchard and field mesocosm cages

449 To mimic the natural surroundings and weather conditions that flies are exposed to in nature, we
450 conducted the study in an experimental orchard at the University of Pennsylvania in
451 Philadelphia. The orchard consisted of cleared land with walk-in mesocosm cages (2m x 2m x
452 2m) constructed of fine mesh and built around metal frames (BioQuip PO 1406C). We planted a
453 dwarf peach tree in each mesocosm cage to provide flies with shade. All peaches were removed

454 before ripening to prevent flies from feeding or laying eggs on them. To provide flies with a
455 feeding and breeding substrate, we added 1.5lb aluminum loaf pans with 400ml Drosophila
456 growth media every two days during the experiment. To avoid an overcrowded developmental
457 environment for the eggs, each loaf pan was covered with a screen mesh lid every two days
458 during the experiment, and eggs were allowed to develop until eclosion ceased, at which point
459 adult flies were released into the general population. The loaf pans were placed on a shelving
460 unit oriented away from direct sunlight to protect them from rain and direct sun.
461
462 Establishment of experimental *D. melanogaster* populations in field mesocosm cages
463 To construct the baseline *D. melanogaster* population for the experiment, we crossed the
464 76 fully sequenced LNPA inbred lines from Pennsylvania. We used inbred lines to facilitate the
465 use of haplotype inference to attain high effective sequencing coverage[29]. To initiate the baseline
466 population, we combined 10 females and 10 males from each line into a single breeding cage.
467 After 4 generations of mating and density-controlled rearing in laboratory conditions, we
468 introduced 500 females and 500 males of a single age cohort into each mesocosm cage on June
469 21, 2021.
470
471 Malathion treatment over the course of the experiment
472 A diagram of the experimental design is shown in **Fig. 3a**. In the first step (*Establishment*
473 *phase*: June 21 to July 20, 2021), we established 20 replicate populations in mesocosm cages and
474 allowed them to expand in the absence of interventions. After establishment, the populations
475 were split into ten malathion-treated and ten malathion-untreated populations. To mimic the
476 insecticide exposure of flies in nature, the malathion-treated populations were exposed to

477 malathion in summer. In nature, insecticides are mainly applied during summer for pest control
478 and their application ceases in the fall[36]. During the malathion treatment phase of the experiment,
479 we sequentially exposed the populations to gradually increasing concentrations of malathion, 1.5
480 - 2.5ppm malathion (July 21 to August 24, 2021) and. 7.5ppm malathion (August 25 to
481 September 6, 2021). We used commercially available malathion grade of 50% strength (Southern
482 Ag Malathion 50% E.C.) and dissolved it in the *Drosophila* growth media. We selected
483 malathion doses based on the Malathion 50% E.C. label instructions to control small insect pests
484 in the field and a previous long-term selection experiment for malathion resistance in *D.*
485 *melanogaster*[37]. The medium supplemented with malathion was prepared once a week to avoid
486 malathion degradation. After the malathion treatment, the experiment lasted until early winter
487 (September 7 to December 22, 2021). Over the course of the experiment, we performed high-
488 resolution temporal sampling (~ bi-weekly sampling during summer and monthly during fall) to
489 track evolution of malathion resistance and genome-wide allele frequencies.
490

491 **Track population size in the field mesocosms over time**

492 To make relative comparisons of population sizes between the malathion-treated and untreated
493 cages, we took photographs of 4 equal size quadrats of the ceiling in each cage at dusk
494 (approximately 2.5% of the ceiling for each quadrat). To count the number of adult flies in each
495 photograph, we designed and validated an algorithm for the semi-automated processing of the
496 photographs. The number of adult flies in each of the 4 photographs was multiplied by 40 to
497 correct for total surface area and obtain 4 population size estimates per cage.
498

499 <u>Statistical analysis of population data</u>

500 To assess the effects of time and malathion treatment on population size, we fitted a linear mixed
501 effect model with the population size estimate as the response variable. We defined our model to
502 investigate the quadratic relationship of time with population size and to account for the random
503 effects attributable to differences in cages. The regression analysis was performed in R (version
504 4.2.2) using lme4 (version 1.1.33).
505
506 **Track malathion resistance in the field mesocosms over time**
507 To characterize the rate and direction of evolution of malathion resistance in the malathion-
508 treated and untreated populations, we repeatedly assayed the evolving populations. Prior to the
509 malathion resistance assay, we collected F1 eggs from each mesocosm cage and transferred them
510 in 2 groups of 200 eggs to bottles with media (i.e., density controlled) in a constant common
511 garden environment (25˚C, 12L:12D, 50% humidity) in the laboratory to distinguish evolution
512 from phenotypic plasticity. We then performed the malathion resistance assay with density and
513 age-controlled individuals from each mesocosm cage in the F2 generation (25˚C, 12L:12D, 50%
514 humidity). The common garden experiment for assaying malathion resistance took place at
515 Stanford University with F1 eggs in bottles with media shipped overnight from the University of
516 Pennsylvania.
517
518 <u>Malathion resistance measurements</u>
519 To characterize the level of malathion resistance in the malathion-treated and untreated
520 populations, we tracked egg to adult survival in the F2 generation on diets that ranged in
521 malathion concentration from 0 ppm to 15 ppm over the course of the experiment. For the
522 collection of F2 eggs, we placed ~ 400 4-to-7-day-old F1 individuals in breeding cages with egg
523 lay caps for 5-7 hours. We then introduced 50 F2 eggs in a narrow vial containing ~7ml of

524 Drosophila growth media supplemented with the range of malathion concentration. We tested
525 each of the malathion concentrations in duplicate vials. We used commercial malathion of 50%
526 strength (Southern Ag Malathion 50% E.C.) and dissolved it in the Drosophila growth media.
527 This medium was kept overnight at 4ºC and used the next day for the assay. We monitored adult
528 eclosion every evening over a period of 10 days until all adult flies had eclosed.
529
530 Statistical analysis of malathion resistance data
531 To assess the temporal dynamics of malathion resistance in both malathion-treated and untreated
532 cages, we fitted separate linear mixed-effects models using the lmer() function in the R package
533 lme4 (version 1.1.33). The response variable in these models was malathion resistance, measured
534 as the LD_{50} value, the dose that causes 50% egg-to-adult mortality. For the malathion-treated
535 cages, we modeled resistance changes over two distinct time periods: (1) from July 26, 2021, to
536 September 21, 2021, when populations were evolving under malathion exposure, and (2) from
537 September 21, 2021, to December 22, 2021, after malathion treatment had ceased. In contrast,
538 for the malathion-untreated cages, we assessed resistance changes over the full experimental
539 period, from July 26, 2021, to December 22, 2021. To avoid biases, we excluded data from July
540 13, 2021, because the LD_{50} estimate from this time point was underestimated due to a technical
541 error. In each model, we included time point as fixed effect, while a random intercept was
542 included for each cage to account for between-cage variability. The main outcome measure of
543 malathion resistance for each cage at each time point was the mean of 1–2 technical replicate
544 LD_{50} measurements. To estimate LD_{50} for each technical replicate per cage per time point, we
545 fitted four-parameter logistic dose-response models using the L.4() function in the drc package

546 (version 3.0.1) in R (version 4.2.2) with egg to adult viability at the range of malathion
547 concentrations as the response variable.
548
549 **Track genome-wide allele frequencies in the field mesocosms over time**
550 To track the trajectories of the resistant and sensitive *Ace* alleles and characterize the extent of
551 the sweep caused by the *Ace* alleles, we tracked genome-wide allele frequencies of the evolving
552 populations across the experiment using the software tool HAF-pipe. HAF-pipe estimates
553 genome-wide allele frequencies in the evolving populations via inference of known founder
554 haplotypes from low-coverage pooled sequencing data [29]. As part of our experimental design, we
555 performed whole-genome, low-coverage pooled sequencing of 100 randomly selected F1
556 females from each of the 20 evolving populations at eight time points through the experiment. To
557 measure biological and technical variation, we performed whole-genome, low-coverage pooled
558 sequencing of different sets of 100 randomly selected F1 females from the 20 evolving
559 populations at two time points collected at Stanford (biological replicates) and of same samples
560 of 100 randomly selected F1 females but processed independently (technical replicates). Last, to
561 evaluate the accuracy of HAF-pipe, we performed whole-genome, high-coverage pooled
562 sequencing of four biological replicate samples from the baseline population and for the evolving
563 populations at an early and a late time point. The data for the untreated cages were also used for
564 a recent independent study from Bitter and colleagues [16].
565
566 <u>Sample collection, DNA extraction, library preparation, and sequencing</u>
567 We collected samples from each population approximately every two generations during
568 the summer phase and every generation during the fall phase. To collect the samples, we placed a
569 new loaf pan with Drosophila growth media in each mesocosm cage one day before collection.

570 The next day, we transferred five groups of 200 F1 eggs to bottles with media, where we
571 controlled the density and maintained them in a constant laboratory environment of 25°C,
572 12L:12D, and 50% humidity. Three bottles with F1 eggs were kept at UPenn and two bottles
573 with F1 eggs were shipped overnight to Stanford. At Stanford, F1 adults were allowed to lay
574 eggs, and 200 F2 eggs were placed in vials for density control. For both the F1 and F2
575 generation, we harvested 4-to-7-day-old individuals after eclosion and preserved them in 100%
576 ethanol in 1.5ml vials at -20°C until further processing.

577 For each sample, we prepared genomic DNA from pools of 100 ethanol-preserved
578 females. We first submerged the samples twice in a rehydration buffer (400 mM NaCl, 20 mM
579 Tris-HCl pH 8.0, 30 mM EDTA) for 15 min at room temperature and then isolated genomic
580 DNA using the Monarch Genomic DNA purification kit (Cat No. 3010L, New England Biolabs).
581 The manufacturer's protocol was modified to include a step for tissue homogenization with two
582 3mm glass beads (Cat No. 11-312C, Fisher Scientific) in a bead beater for five minutes to ensure
583 complete homogenization of the flies so that the genomic DNA from each fly was equally
584 represented in the genomic DNA pool. We quantified the genomic DNA using the Qubit dsDNA
585 BR (Broad-Range) Assay kit (Cat No. Q32853, Life Technologies) on a Qubit
586 spectrophotometer and estimated its purity on a NanoDrop spectrophotometer.

587 We then prepared sequencing libraries using the Illumina DNA prep, (M) Tagmentation
588 kit (Cat No. 20018705, Illumina Inc.) and the Illumina UD Indexes sets (Cat No 20027123,
589 20027214, 20042666, 20042667, Illumina Inc.) for unique dual indexing. We modified the
590 manufacturer's protocol by preparing libraries in 1/5 of the recommended reaction volume to
591 maximize kit efficiency and pooling equimolarly amplified libraries in sets of eight after the
592 library amplification step. After the cleanup, we quantified the pooled libraries using a Qubit

593 spectrophotometer and an Agilent Bioanalyzer. Finally, the pooled libraries were 150bp paired-
594 end sequenced on the NovaSeq 6000 S2 platform at the Sequencing Service Center at the
595 Stanford Genomics Center and on a NovaSeq 6000 SP platform at Admera. All sequences will
596 be deposited in SRA.
597
598 Processing of DNA sequencing data for genome-wide allele frequency estimation
599 We trimmed the raw sequencing reads of adapter sequences and bases with quality score
600 < 20. We then mapped the trimmed reads to the *D. melanogaster* reference genome (v5.39) using
601 bwa and default parameters [38], and aligned reads were deduplicated using Picard tools. We
602 randomly sampled reads from the aligned bams to obtain an equivalent, genome-wide coverage
603 of 8x across all samples. We computed haplotype-derived allele frequency (HAF) estimates
604 using HAF pipe. Briefly, after using an expectation-maximization algorithm to estimate
605 haplotype frequencies in overlapping genomic windows from mapped sequence reads (originally
606 developed by Kessner and colleagues [39]) at each site previously identified as polymorphic in the
607 inbred reference panel, we summed the estimated frequencies of haplotypes carrying the
608 alternate allele to obtain HAFs . We conducted haplotype inference in window sizes that varied
609 proportionally to the expected length of un-recombined haplotype blocks, which varied as a
610 function of the estimated number of generations since the original outbreeding. HAFs were
611 compiled to only include those sites with an average minor allele frequency (MAF) > 0.02 in the
612 baseline population, and present in at least one evolved sample at a MAF > 0.01.
613

614 **Track trajectories of sensitive and resistant *Ace* alleles in the evolving populations over**
615 **time**

616 We first estimated the frequency of each of the 76 founder haplotypes in the *Ace* region
617 (Chr3R:9,063,921-9,069,721) in each of the malathion-treated and malathion-untreated
618 populations at each time point, focusing on the founders containing the four known resistance
619 mutations . To obtain an accurate measure of the frequency of each haplotype, we calculated the
620 mean frequency across the 10 overlapping genomic windows that included each site within the
621 region of interest.

622 We then estimated the relative frequency of each *Ace* allele, defined by the combination
623 of the four known resistance mutations, in each population at each time point. Given our
624 knowledge of the resistance mutation combinations for each founder, we computed the relative
625 frequency of each *Ace* allele (Ace-S: IGFG, Ace-R1: VGFG, Ace-R2: VGFA, Ace-R3: VAYG,
626 Ace-R4:IGFA, Ace-R5:IGYG, Ace-R6:VAFG, Ace-R7: VAYA) by summing the frequencies of
627 the haplotype blocks from the 76 founders that shared the same *Ace* allele. For founders
628 heterozygous for the *Ace* alleles, we divided the contributions of their haplotype block evenly
629 between the two corresponding *Ace* allele frequencies. *Ace* alleles with a frequency < 0.01%
630 (Ace-R4:IGFA, Ace-R5:IGYG, Ace-R6:VAFG, Ace-R7: VAYA) in the evolving populations
631 were excluded from further analysis.

632

633 Statistical analysis of *Ace* allele frequency data

634 To assess the temporal dynamics of *Ace* allele frequencies (Ace-S: IGFG, Ace-R1:
635 VGFG, Ace-R2: VGFA, Ace-R3: VAYG), we fitted separate linear mixed-effects models using
636 the lmer() function in the R package lme4 (version 1.1.33). The response variables in these

637 models were the frequencies of each *Ace* allele. For the malathion-treated cages, we modeled *Ace*
638 allele frequency changes over two distinct time periods: (1) from July 26, 2021, to September 21,
639 2021, when populations were evolving under malathion exposure, and (2) from September 21,
640 2021, to December 22, 2021, after malathion treatment had ceased. In contrast, for the
641 malathion-untreated cages, we assessed *Ace* allele frequency changes from the beginning of the
642 treatment to the end of the experiment, from July 26, 2021 to December 22, 2021.
643

644 **Model *Ace* allele frequency evolution**

645 We simulated the evolution of *Ace* allele frequencies and malathion resistance in our mesocosm
646 experiments using a viability selection model[40]. Additionally, based on the changes in *Ace* allele
647 frequencies in malathion-free environments across both sets of cages, we estimated the possible
648 ranges for the fitness costs of and dominance of malathion resistance.
649

650 <u>The impact of viability on *Ace* allele frequency dynamics and malathion resistance in the field</u>
651 <u>mesocosm experiment</u>

652 We investigated whether selection acting on viability recapitulates the allele frequency
653 and malathion resistance dynamics observed in the field. We focused on viability as it is a key
654 fitness-related trait in both malathion-rich and malathion-free environments. Furthermore, we
655 had laboratory measurements of viabilities for *Ace* genotypes across ranges of malathion
656 concentrations, allowing us to parametrize our model and test its predictions.
657 Within our model, the population frequencies of the *Ace* alleles change only due to selection that
658 acts on viability. We assumed that the effects of other forces (mutation, recombination, and
659 genetic drift) were negligible in comparison over the timescales that we considered (~10

660 generations). Under these assumptions, the frequency dynamics of the sensitive (f_0) and resistant

661 (f_1, f_2, f_3) *Ace* alleles follow from

662 $$f_i(t+1) = \frac{f_i(t)\sum_j w_{ij} f_j(t)}{\overline{w}(t)},$$

663 where t is time measured in generations, w_{ij} is viability of individuals carrying both i and j

664 alleles, and $\overline{w}$ is the mean population viability defined as

665 $$\overline{w}(t) = \sum_{i,j} f_i(t) f_j(t) w_{ij}.$$

666 We used laboratory measurements to determine individual viabilities w_{ij} in the absence

667 and presence of malathion (at 2.5 and 7.5 ppm). We used the marginal mean values from the

668 linear model for viability for each genotype and the predicted viability values from the dose-

669 response analysis (see previous section on 'Statistical analysis of fitness-associated phenotypes').

670 Due to the lack of measurements for heterozygous resistant genotypes, we assumed that

671 combinations of resistant alleles are codominant, i.e. that $w_{12} = 0.5 \cdot w_{11} + 0.5 \cdot w_{22}$; $w_{13} = 0.5 \cdot$

672 $w_{11} + 0.5 \cdot w_{33}$; $w_{23} = 0.5 \cdot w_{22} + 0.5 \cdot w_{33}$. The initial *Ace* allele frequencies, $f_i(0)$, were

673 estimated as the median values from the first sampling time point (July 13, 2021) for each

674 treatment group.

675 To estimate *D. melanogaster* generation times at our eight sampling time points, we used

676 a degree-day model based on Behrman and Schmidt[41]. This model assumes *D. melanogaster*

677 requires 112 degree-days to complete one generation, with development occurring between 12°C

678 and 29°C. We calculated daily degree-days as [(daily max. temp. + daily min. temp.) / 2] - 12°C,

679 adjusting temperatures outside the 12-29°C range to these limits. Cumulative degree-days were

680 tracked, with each 112 degree-day accumulation marking a new generation. This allowed us to

681 estimate generations at each sampling time point throughout the experiment.

682 We then calculated the population resistance R as a weighted sum,

683 $$R(t) = \sum_{i,j} g_{ij}(t) w_{ij},$$

684 where $g_{ij}(t)$ are genotype frequencies and w_{ij} are the corresponding viabilities. The initial

685 genotype frequencies were estimated from the initial allele frequencies, assuming Hardy-

686 Weinberg equilibrium:

687 $$g_{ij}(0) = f_i(0) f_j(0).$$

688 The consequent genotype frequencies followed from the viability selection model,

689

690 $$g_{ij}(t) = \begin{cases} \frac{2 f_i(t) f_j(t) w_{ij}}{\overline{w}}, i \neq j, \\ \frac{f_i(t) f_j(t) w_{ij}}{\overline{w}}, i = j. \end{cases}$$

691

692 <u>Inferring the ranges of possible fitness costs and dominance coefficients from empirical allele</u>

693 <u>frequency trajectories</u>

694 To estimate the fitness cost and dominance of malathion resistance in the malathion-free

695 environment, we analyzed the empirical frequency trajectories of these alleles in both the

696 untreated and treated populations after the removal of malathion. This approach allowed us to

697 constrain the range of possible parameters that could explain the observed frequencies of the

698 resistant alleles in both the treated and untreated populations. Assuming the resistant alleles share

699 the same selection (s) and dominance (h) coefficients, and further that the cost of resistance is

700 small (s<<1), the frequency dynamics follow

701 $$\partial_t f = s(f \cdot (\mathbf{1} - f) \cdot (f + \boldsymbol{h}(\mathbf{1} - \mathbf{2} f))),$$

702 allowing us to find s that would be consistent with the observed slope $\partial_t f$ of the frequency

703 trajectory for a given h[42].

704 To do that, we first bootstrapped the combined frequency trajectories of resistant alleles

705 in individual cages within each treatment group 10,000 times. For each set of bootstrapped

706 trajectories, we used linear regression (LinearRegression().fit function from the scikit-learn

707 Python library[43] to infer their slope. For a range of $h \in [0,1]$, we then calculated the bounds on s
708 by finding the values that correspond to the lower and upper bound of the 95% confidence
709 interval of the bootstrap distribution. To further constrain the range of possible parameters, we
710 similarly inferred the full distribution of s for each set of cages, and evaluated their overlap by
711 computing the joint likelihood function,

712 $$\mathcal{L} = \prod p(s),$$

713 where $p(s)$ is the probability density corresponding to a fixed value of s. Larger values of L
714 therefore correspond to more likely combinations of h and s given the observed frequency
715 dynamics.
716

717 **Characterize extent of forward and reverse sweep caused by *Ace* resistant alleles**

718 To assess how fluctuating organophosphate selection on the R2 and R3 *Ace* resistant alleles
719 affected genome-wide frequency trajectories of linked SNPs during and post-malathion
720 treatment, we employed a two-step approach. First, we used quasibinomial logistic regression to
721 estimate allele frequency shifts for genome-wide SNPs during malathion treatment (July 26 to
722 September 21, 2022) and post-treatment (September 21 to December 22, 2021). Second, we
723 developed a linked SNP selection procedure using linkage information from the inbred lines to
724 identify SNPs tightly linked (Ace-linked) and loosely linked (control) to the sweeping R2 and R3
725 *Ace* alleles across the genome. We used these sets of SNPs to quantify the extent of both the
726 forward *Ace* sweep during malathion treatment and the reverse *Ace* sweep post-treatment.
727

728 <u>Quasi-binomial logistic regression to estimate allele frequency differences in malathion-treated</u>
729 <u>and untreated populations during and after the malathion treatment</u>

730 To quantify allele frequency changes during malathion treatment (July 26 to September
731 21, 2022) and post-treatment (September 21 to December 22, 2021) in both treated and untreated
732 populations, we used a quasibinomial logistic regression approach[14,44]. This method models the
733 number of reads mapped to the alternative allele 'α' (relative to the reference allele 'A') at each
734 biallelic SNP for each pooled sample. To account for both the expected accuracy of HAFs as
735 well as pseudo-replication due to a fixed number of individuals in each sample [45], we estimated
736 an effective read depth reads (at each biallelic SNP for each pooled sample per population using
737

738 $$n_{eff} = \frac{\left((2 \times N \times EC) - 1\right)}{2 \times N + EC}$$

739

740 where N is the number of individuals per sample (100) and EC is the expected effective read
741 coverage based on the accuracy of HAF-pipe.
742 We then used a logit link implemented in a quasi-binomial logistic regression to model the
743 counts of the alternative allele 'α' $(C_a = HAF * neff)$ and reference allele 'A' $(C_A = (1 -$
744 $HAF) * neff)$ as a function of time in the malathion-treated and -untreated populations
745

746 $$logit(p_a) = log\left(\frac{p_a}{1 - p_a}\right) = b_0 + b_1 \times time + e$$

747 where p_a is probability of observing the allele 'α', while the coefficients b_0 and b_1 correspond to
748 the intercept and the effect of time, respectively. We fitted the model using the glm() function in
749 R (version 4.2.2) with family = 'quasibinomial'. To compute the allele frequency change (effect
750 size) between two time points (x_1 and x_2), we calculated

751 $$\Delta p = p_2 - p_1 = \frac{e^{(b_0 + b_1 \times x_2)}}{1 + e^{(b_0 + b_1 \times x_2)}} - \frac{e^{(b_0 + b_1 \times x_1)}}{1 + e^{(b_0 + b_1 \times x_1)}}$$

752

753 Analysis of allele frequency changes of Ace-linked SNPs

754 To quantify the extent of the forward *Ace* sweep during malathion treatment, we
755 identified SNPs linked to the sweeping R2 and R3 *Ace* alleles, as well as unlinked (control)
756 SNPs, using whole genome data from the 76 sequenced Pennsylvania inbred lines (LNPA). First,
757 we labeled R2 and R3 *Ace* alleles as "R" and the remaining alleles (R1 and S) as "S", creating a
758 binary "R"/"S" *Ace* locus across the inbred lines. Among the inbred lines, 54 were homozygous
759 "S", 5 heterozygous "R/S", and 17 homozygous "R". To select linked SNPs, we used the inbred
760 lines data to compute r2 between the binary "R"/"S" *Ace* locus and every reported biallelic SNP
761 in the inbred LNPA lines as the squared correlation coefficient of allelic indicator variables[46].
762 We initially retained SNPs with r2 > 0.03, a threshold frequency previously used to deem two
763 loci highly linked[16]**.** However, to avoid issues with low-frequency SNPs in finite populations, we
764 added an allele count condition. We selected SNPs with r2 > 0.03 that also have an allele present
765 in ≥60% of "R/R" lines and in ≤40% of “S/S” and “S/R” lines. This ensures selection of high-
766 frequency, well-assorted SNPs between "R" and "S" lines, which are more informative for sweep
767 analysis. This approach yielded 5672 Ace-linked SNPs across chromosomes 2, 3, and X. The
768 60% threshold was chosen as the highest value providing enough Ace-linked SNPs to uniformly
769 cover the genome, with consistent results when varied. Finally, for each Ace-linked SNP, we
770 selected an unlinked control SNP with r2 < 0.01 with the binary "R"/"S" *Ace* locus. To ensure
771 comparable initial conditions, unlinked control SNPs were chosen within 500kb of their linked
772 counterpart and had an allele frequency within 0.05 of the Ace-linked SNP at the start of
773 malathion treatment in each cage. This process yielded 4793 matched unlinked control SNPs,
774 fewer than the linked SNPs due to the stringent matching criteria. To visualize the results, we

775 aggregated SNPs into 500kb windows along the genome and used bootstrap resampling to
776 compute median GLM-estimated effect sizes and confidence intervals for Ace-linked and
777 unlinked control SNPs separately. To statistically characterize the width of the forward sweep,
778 for each of the 100,000 bootstrap samples, we have identified the range of windows on the 3R
779 arm on which the median for linked SNPs is larger than the median for the control SNPs, and
780 recorded the width of the positive range, resulting in a bootstrap sample of sweep widths.

781 To quantify the reverse *Ace* sweep post-malathion treatment, we analyzed allele
782 frequency changes for the same Ace-linked and unlinked control SNPs during the post-treatment
783 period (September 21 to December 22, 2021). We compared post-treatment to during-treatment
784 frequency changes, plotting them against each other while considering genomic distance from
785 the *Ace* locus on chromosome 3R. To quantify this relationship, we analyzed the correlation
786 between these changes as a function of distance from *Ace*. We used 500kb windows and
787 bootstrap resampling to compute median effect sizes and confidence intervals for Ace-linked and
788 unlinked control SNPs, consistent with our forward sweep analysis approach.

789 **References**

790

791 1. Dobzhansky, T. A review of some fundamental concepts and problems of population
792 genetics. *Cold Spring Harb. Symp. Quant. Biol.* **20**, 1–15 (1955).
793 2. Hedrick, P. W. Genetic polymorphism in heterogeneous environments: The age of
794 genomics. *Annu. Rev. Ecol. Evol. Syst.* **37**, 67–93 (2006).
795 3. Hedrick, P. W. Genetic variation in a heterogeneous environment. II. Temporal
796 heterogeneity and directional selection. *Genetics* **84**, 145–157 (1976).
797 4. Wittmann, M. J., Bergland, A. O., Feldman, M. W., Schmidt, P. S. & Petrov, D. A.
798 Seasonally fluctuating selection can maintain polymorphism at many loci via segregation
799 lift. *Proc. Natl. Acad. Sci. U. S. A.* **114**, E9932–E9941 (2017).
800 5. Posavi, M., Gelembiuk, G. W., Larget, B. & Lee, C. E. Testing for beneficial reversal of
801 dominance during salinity shifts in the invasive copepod Eurytemora affinis, and
802 implications for the maintenance of genetic variation: TESTING FOR REVERSAL OF
803 DOMINANCE. *Evolution* **68**, 3166–3183 (2014).
804 6. Di, C. & Lohmueller, K. E. Revisiting dominance in population genetics. *Genome Biol.*
805 *Evol.* **16**, 1–17 (2024).
806 7. Menozzi, P., Shi, M. A., Lougarre, A., Tang, Z. H. & Fournier, D. Mutations of
807 acetylcholinesterase which confer insecticide resistance in Drosophila melanogaster
808 populations. *BMC Evol. Biol.* **4**, 4 (2004).
809 8. Wright, S. Physiological and evolutionary theories of dominance. *Am. Nat.* **68**, 24–53
810 (1934).
811 9. Brian, C. & Hugues, K. A. The maintenance of genetic variation in life-history traits. in

812 *Evolutionary genetics* (eds. Singh, R. S. & Krimbas, C. B.) 369–392 (Cambridge University
813 Press, Cambridge, England, 2000).
814 10. Charlesworth, B. Causes of natural variation in fitness: evidence from studies of Drosophila
815 populations. *Proc. Natl. Acad. Sci. U. S. A.* **112**, 1662–1669 (2015).
816 11. Hedrick, P. W. Balancing selection. *Curr. Biol.* **17**, R230–1 (2007).
817 12. Bergland, A. O., Behrman, E. L., O'Brien, K. R., Schmidt, P. S. & Petrov, D. A. Genomic
818 evidence of rapid and stable adaptive oscillations over seasonal time scales in Drosophila.
819 *PLoS Genet.* **10**, e1004775 (2014).
820 13. Machado, H. E. *et al.* Broad geographic sampling reveals the shared basis and
821 environmental correlates of seasonal adaptation in Drosophila. *Elife* **10**, (2021).
822 14. Rudman, S. M. *et al.* Direct observation of adaptive tracking on ecological time scales in
823 Drosophila. *Science* **375**, eabj7484 (2022).
824 15. Pfenninger, M. & Foucault, Q. Population genomic time series data of a natural population
825 suggests adaptive tracking of fluctuating environmental changes. *Integr. Comp. Biol.* **62**,
826 1812–1826 (2022).
827 16. Bitter, M. C. *et al.* Continuously fluctuating selection reveals fine granularity of adaptation.
828 *Nature* **634**, 389–396 (2024).
829 17. Curtsinger, J. W., Philip M. Service & Prout, T. Antagonistic pleiotropy, reversal of
830 dominance, and genetic polymorphism. *Am. Nat.* **144**, 210–228 (1994).
831 18. Hall, J. C. & Kankel, D. R. Genetics of acetylcholinesterase in Drosophila melanogaster.
832 *Genetics* **83**, 517–535 (1976).
833 19. Aldridge, W. N. Some properties of specific cholinesterase with particular reference to the
834 mechanism of inhibition by diethyl p-nitrophenyl thiophosphate (E 605) and analogues.

835 *Biochem. J.* **46**, 451–460 (1950).

836 20. Miyo, T., Akai, S. & Oguma, Y. Seasonal fluctuation in susceptibility to insecticides within
837 natural populations of Drosophila melanogaster: empirical observations of fitness costs of
838 insecticide resistance. *Genes Genet. Syst.* **75**, 97–104 (2000).

839 21. Miyo, T., Oguma, Y. & Charlesworth, B. Seasonal fluctuation in susceptibility to
840 insecticides within natural populations of Drosophila melanogaster. II. Features of genetic
841 variation in susceptibility to organophosphate insecticides within natural populations of D.
842 melanogaster. *Genes Genet. Syst.* **81**, 273–285 (2006).

843 22. Karasov, T., Messer, P. W. & Petrov, D. A. Evidence that adaptation in Drosophila is not
844 limited by mutation at single sites. *PLoS Genet.* **6**, e1000924 (2010).

845 23. Mackay, T. F. C. *et al.* The Drosophila melanogaster Genetic Reference Panel. *Nature* **482**,
846 173–178 (2012).

847 24. Kapun, M. *et al.* Drosophila Evolution over Space and Time (DEST): A new population
848 genomics resource. *Mol. Biol. Evol.* **38**, 5782–5805 (2021).

849 25. Shi, M. A. *et al.* Acetylcholinesterase alterations reveal the fitness cost of mutations
850 conferring insecticide resistance. *BMC Evol. Biol.* **4**, 5 (2004).

851 26. Langmüller, A. M. *et al.* Fitness effects for Ace insecticide resistance mutations are
852 determined by ambient temperature. *BMC Biol.* **18**, 157 (2020).

853 27. Paaby, A. B., Bergland, A. O., Behrman, E. L. & Schmidt, P. S. A highly pleiotropic amino
854 acid polymorphism in the Drosophila insulin receptor contributes to life-history adaptation.
855 *Evolution* **68**, 3395–3409 (2014).

856 28. Bitter, M. C. *et al.* Continuously fluctuating selection reveals extreme granularity and
857 parallelism of adaptive tracking. *bioRxivorg* (2024) doi:10.1101/2023.10.16.562586.

858 29. Tilk, S. *et al.* Accurate Allele Frequencies from Ultra-low Coverage Pool-Seq Samples in
859 Evolve-and-Resequence Experiments. *G3* **9**, 4159–4168 (2019).
860 30. Taverner, A. M. *et al.* Adaptive substitutions underlying cardiac glycoside insensitivity in
861 insects exhibit epistasis in vivo. *Elife* **8**, (2019).
862 31. Guo, L. *et al.* Convergent resistance to GABA receptor neurotoxins through plant-insect
863 coevolution. *Nat. Ecol. Evol.* **7**, 1444–1456 (2023).
864 32. Wittmann, M. J., Mousset, S. & Hermisson, J. Modeling the genetic footprint of fluctuating
865 balancing selection: from the local to the genomic scale. *Genetics* **223**, iyad022 (2023).
866 33. Mutero, A., Pralavorio, M., Bride, J. M. & Fournier, D. Resistance-associated point
867 mutations in insecticide-insensitive acetylcholinesterase. *Proc. Natl. Acad. Sci. U. S. A.* **91**,
868 5922–5926 (1994).
869 34. Harel, M. *et al.* Three-dimensional structures of Drosophila melanogaster
870 acetylcholinesterase and of its complexes with two potent inhibitors. *Protein Sci.* **9**, 1063–
871 1072 (2000).
872 35. Ritz, C., Baty, F., Streibig, J. C. & Gerhard, D. Dose-Response Analysis Using R. *PLoS*
873 *One* **10**, e0146021 (2015).
874 36. Miyo, T. & Oguma, Y. Negative correlations between resistance to three organophosphate
875 insecticides and productivity within a natural population of Drosophila melanogaster
876 (Diptera: Drosophilidae). *J. Econ. Entomol.* **95**, 1229–1238 (2002).
877 37. Singh, R. S. & Morton, R. A. Selection for malathion-resistance in Drosophila
878 melanogaster. *Can. J. Genet. Cytol.* **23**, 355–369 (1981).
879 38. Li, H. & Durbin, R. Fast and accurate short read alignment with Burrows-Wheeler
880 transform. *Bioinformatics* **25**, 1754–1760 (2009).

881 39. Kessner, D., Turner, T. L. & Novembre, J. Maximum likelihood estimation of frequencies
882 of known haplotypes from pooled sequence data. *Mol. Biol. Evol.* **30**, 1145–1158 (2013).
883 40. Gillespie, J. H. *Population Genetics*. (Johns Hopkins University Press, Baltimore, MD,
884 2004).
885 41. Behrman, E. L. & Schmidt, P. How predictable is rapid evolution? (2022)
886 doi:10.1101/2022.10.27.514123.
887 42. Ewens, W. J. *Mathematical Population Genetics 1: Theoretical Introduction*. (Springer,
888 New York, NY, 2010).
889 43. Pedregosa, F. *et al.* Scikit-learn: Machine Learning in Python. *arXiv [cs.LG]* (2012).
890 44. Wiberg, R. A. W., Gaggiotti, O. E., Morrissey, M. B. & Ritchie, M. G. Identifying
891 consistent allele frequency differences in studies of stratified populations. *Methods Ecol.*
892 *Evol.* **8**, 1899–1909 (2017).
893 45. Feder, A. F., Petrov, D. A. & Bergland, A. O. LDx: estimation of linkage disequilibrium
894 from high-throughput pooled resequencing data. *PLoS One* **7**, e48588 (2012).
895 46. VanLiere, J. M. & Rosenberg, N. A. Mathematical properties of the r2 measure of linkage
896 disequilibrium. *Theor. Popul. Biol.* **74**, 130–137 (2008).

Extended Data Figure 1

a

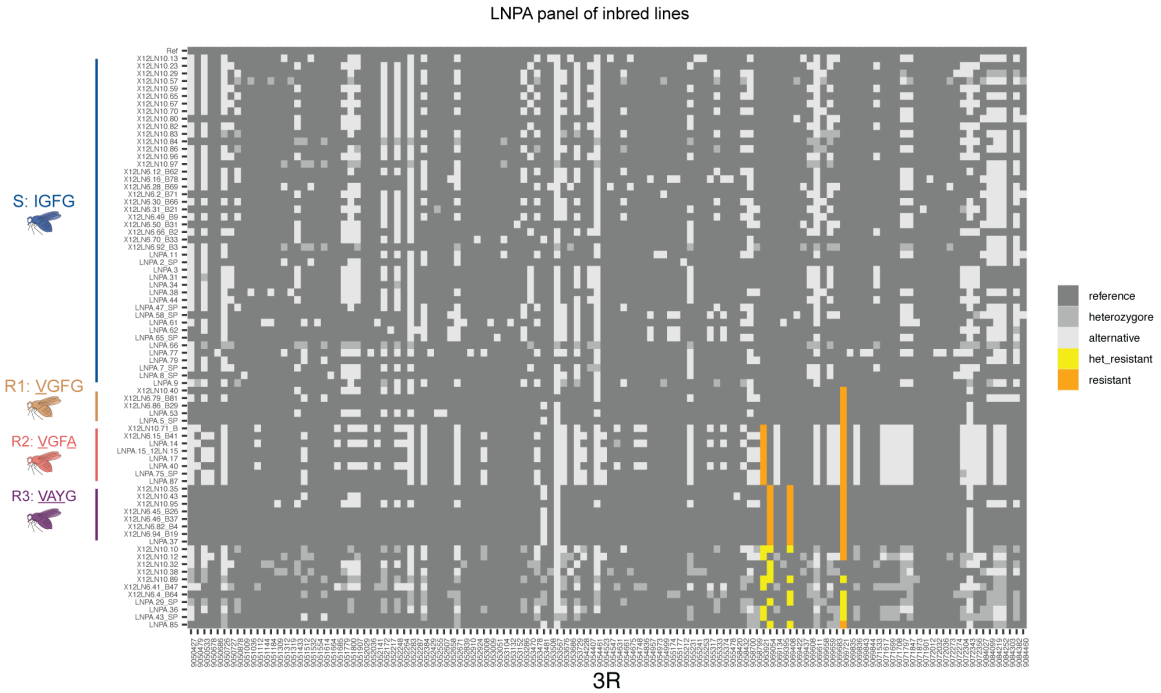

b

Ace haplotype	LNPA relative frequency (%)	DGRP relative frequency (%)
IGFG	63.16	54.15
VGFA	13.16	0.49
VAYG	12.50	30.73
VGFG	7.89	12.20
IGYG	1.32	0.98
IGFA	0.66	NA
VAFG	0.66	NA
VAYA	0.66	NA
IAFG	NA	1.46

Extended Data Figure 1. Sensitive and resistant *Ace* alleles in the panel of LNPA and DGRP inbred lines. a, Heatmap showing clustering of seventy-six *D. melanogaster* isogenic lines in the LNPA panel based on the sensitive or resistant *Ace* allele they carry (Ace-S: IGFG, Ace-R1: VGFG, Ace-R2: VGFA, Ace-R3: VAYG). The x-axis in the heatmap shows the genomic position on chromosome 3R around the *Ace* locus. Each row represents the *Ace* haplotype information of one isogenic line. Each column represents one biallelic exonic SNP at the *Ace* locus. Reference alleles are colored in dark grey, alternative alleles are colored in light grey, heterozygotes in medium grey. For the resistance mutations, alleles coding for the resistance mutations are colored in orange, alternative in grey, and heterozygotes in yellow. **b,** Table showing frequency of the sensitive and each of the resistant *Ace* alleles carrying different resistance haplotypes in the panels of LNPA and DGRP inbred lines.

Extended Data Figure 2

a

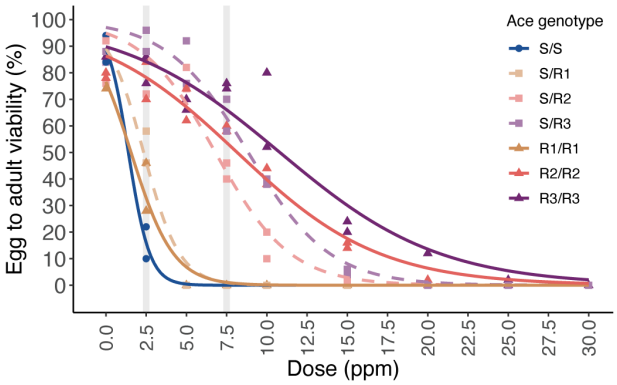

b

Dose response curve analysis for each Ace genotype

Genotype	LD50	std.error	statistic	p.value
SS	1.39	0.18	7.79	3.7768e-12
R1R1	1.56	0.20	7.68	6.3407e-12
R2R2	8.16	0.40	20.41	7.7563e-40
R3R3	10.81	0.45	23.96	3.3625e-46
SR1	2.34	0.19	12.49	3.0000e-23
SR2	6.80	0.26	25.89	2.1374e-49
SR3	8.84	0.30	29.95	1.3764e-55

Extended Data Figure 2. Comparison of malathion resistance among the *Ace* genotypes. a, Lab measurements of egg to adult viability in recombinant populations carrying different *Ace* genotypes on standard Drosophila media with a range of malathion concentrations (n= 2 technical replicates per genotype for each malathion doses, 50 eggs per replicate). Four-parameter logistic models fitted to data of each *Ace* genotype. The shaded areas highlight viability of each genotype at malathion doses (2.5ppm and 7.5 ppm) applied in the field mesocosm experiment. **b,** Table with estimated LD_{50} values for each *Ace* genotype from four-parameter logistic dose-response model (see also **Methods**).

Extended Data Figure 3

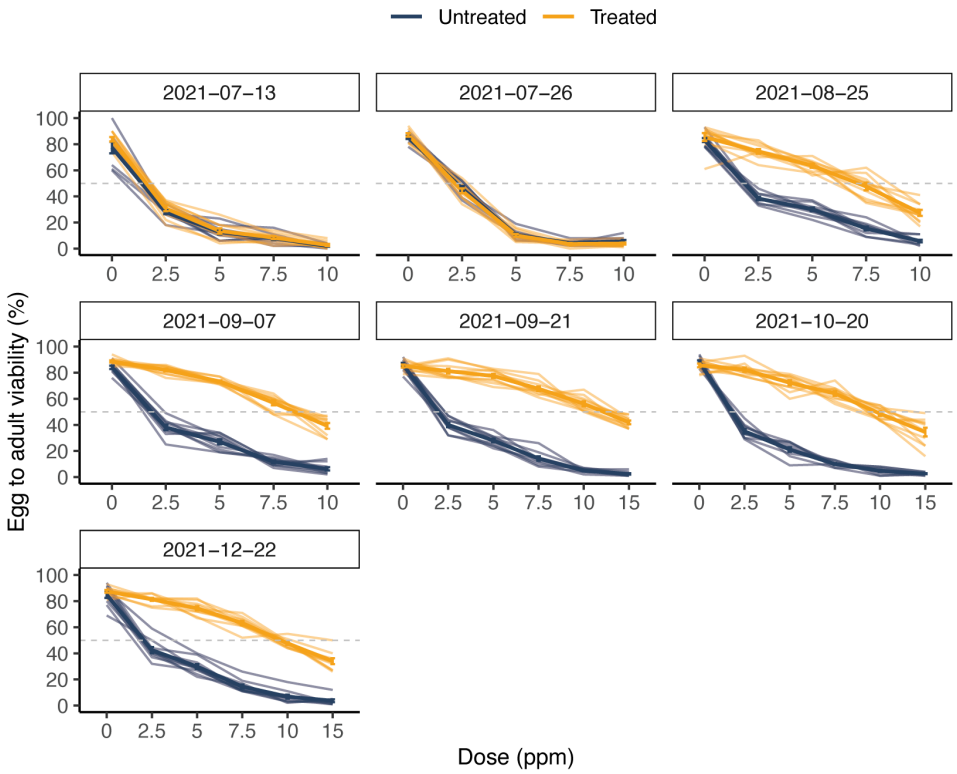

Extended Data Figure 3. Tracking evolution of malathion resistance in the field mesocosm experiment. Egg-adult survival on diets with a range of malathion concentrations as measured after two generations of common garden rearing throughout the field mesocosm experiment. Light lines and points show the mean egg-adult survival for individual malathion-treated (orange) and untreated (blue) populations (n = 2 technical replicates, 50 eggs per replicate). Dark lines and points represent the mean ± s.e.m. from all populations for each treatment group (n = 10 populations per treatment group). Further information on experimental design can be found in **Methods**.

Extended Data Figure 4

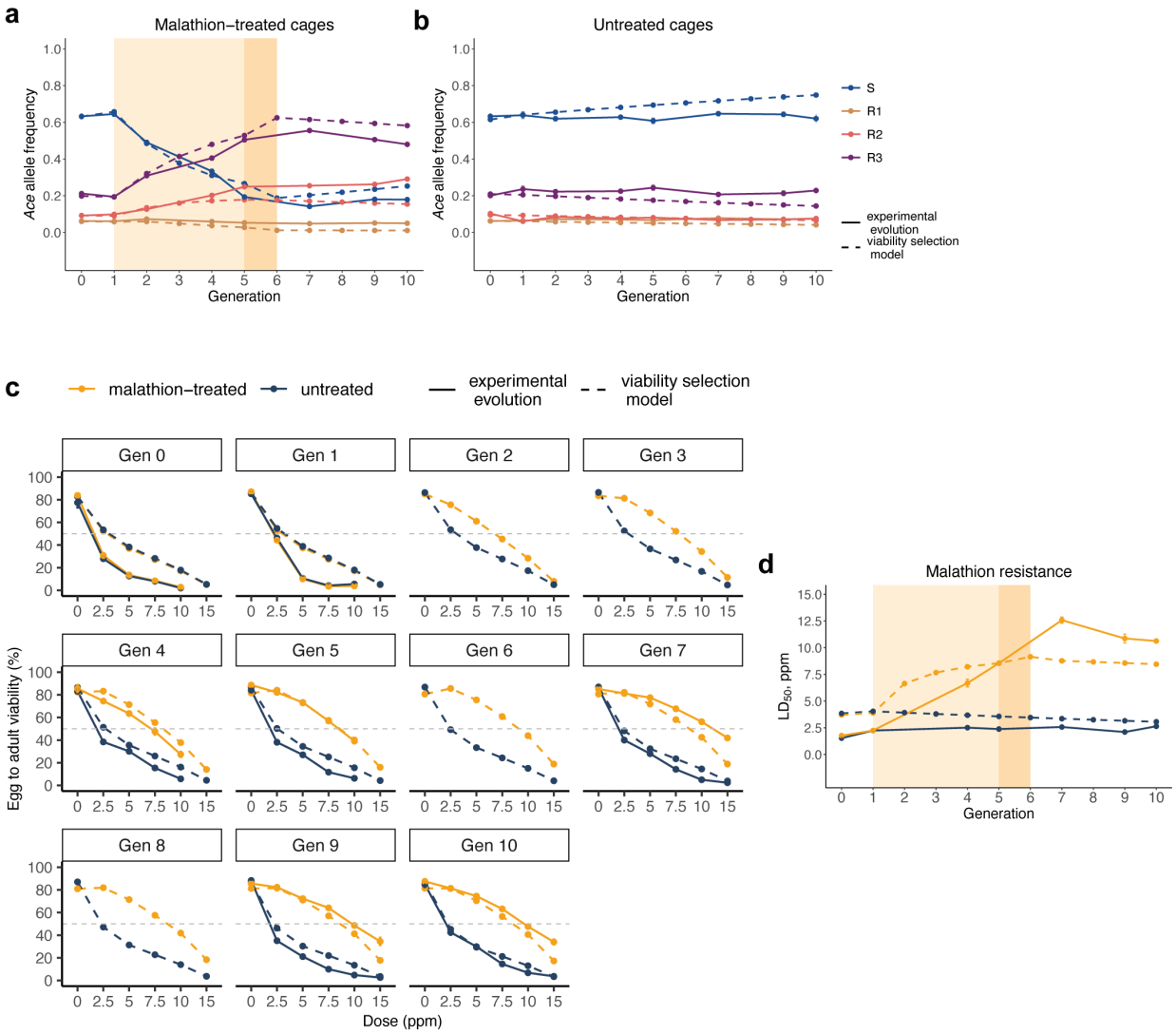

903

Extended Data Figure 4. Modeling the impact of viability selection on *Ace* allele frequency dynamics and malathion resistance in the field mesocosm experiment. **a-b,** Comparison between the observed *Ace* allele frequency trajectories over 10 generations in the malathion-treated (**a**) and untreated (**b**) populations from the field mesocosm experiment (mean ± s.e.m.) and the expected trajectories from simulations based on a viability selection model using laboratory-derived parameters. See **Methods** for details about the viability selection model. **c-d,** Comparison between the observed egg-to-adult survival across a range of malathion concentrations (**c**) and the evolution of malathion resistance (LD_{50}, ppm) (**d**) over 10 generations in the field mesocosm experiment (mean ± s.e.m.), and the expected results from the same model simulations. Dashed lines represent the expected values from the viability selection model, while solid lines represent the observed data from the field experiment. Generations were estimated based on a degree-day model starting from the first sampling point (July 13, 2021). In all plots, points correspond to each generation and estimated time point, and are connected by lines for visualization.

904

Extended Data Figure 5

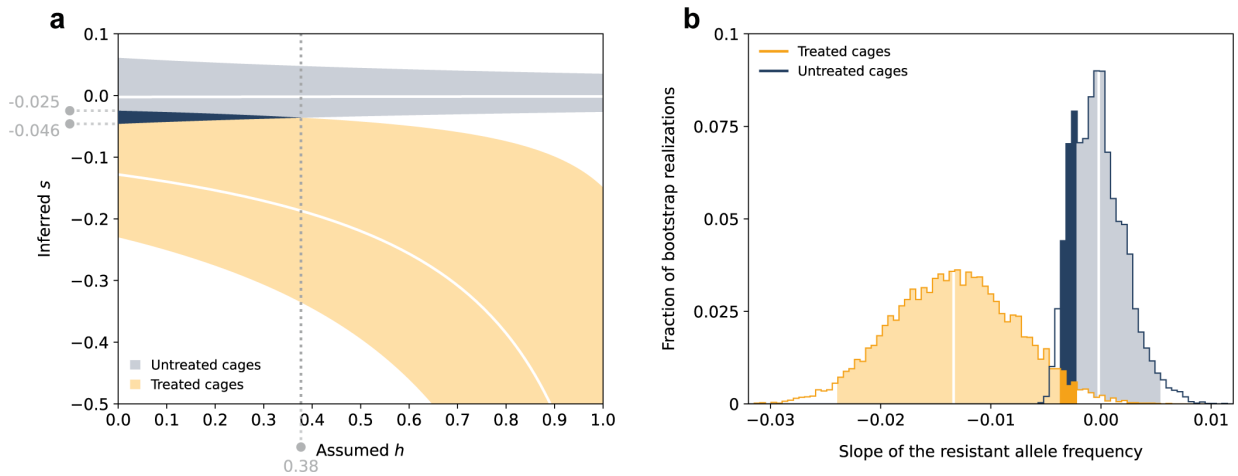

Extended Data Figure 5. Modeling the cost of resistant *Ace* alleles in malathion-free environment. a, Inferred values of the fitness effect of resistance (s) and the dominance coefficients (h) from the change in mutant allele frequencies in treated (orange) and untreated (blue) populations under a viability selection model (see **Methods**). The solid lines correspond to the values of s and h inferred from the mean slope of frequency trajectories, obtained by bootstrapping cages 10,000 times, and the shaded regions denote the values of s and h that lie within the 0.95 confidence region of the bootstrap distribution. All mutants were assumed to share the fitness cost and the dominance coefficient. **b,** The distribution of the slopes of resistant allele frequency trajectories in treated (orange) and untreated (blue) populations, obtained by bootstrapping cages 10,000 times. For each bootstrap realization, the slope was inferred using linear regression. The vertical lines denote the means of the distributions, and the shaded regions correspond to 0.95 confidence intervals.

Extended Data Figure 6

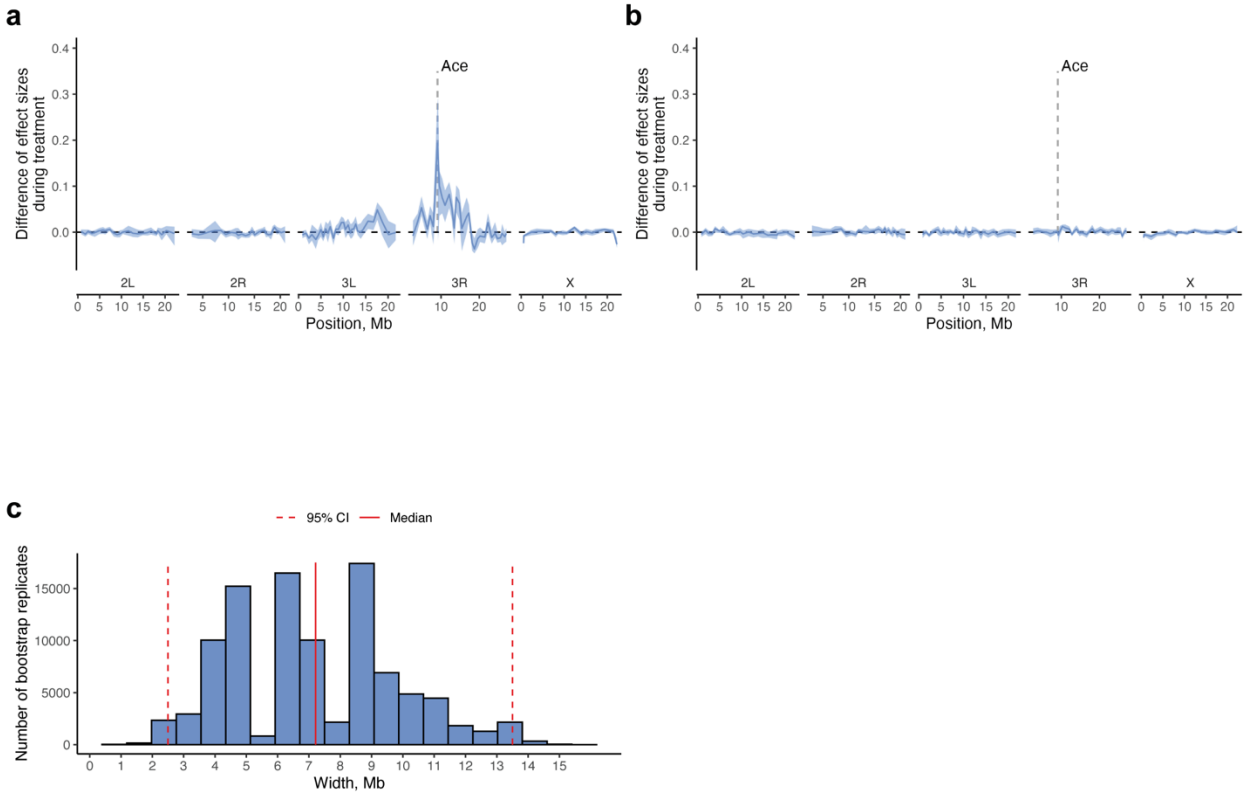

907

Extended Data Figure 6. Characterization of the forward sweep during malathion treatment. a,b, Difference in absolute glm-estimated effect sizes between Ace-linked and unlinked control SNPs in malathion-treated (**a**) and untreated (**b**) cages. Shared areas on the plots represent 95% bootstrap confidence intervals of the difference computed by sampling SNPs in 500kb windows. **c,** Bootstrap sampling distribution of forward sweep width on the 3R arm in the malathion-treated population.

908

Extendend Data Table 1

Effect estimates from linear model analysis for LD50

Parameter	LD50	Std.Error	P.value
SS mean	1.39	0.19	-
SR1 mean	2.34	0.13	-
R1R1 mean	1.56	0.14	-
SS vs. SR1	-0.93	0.34	0.0063
SS vs. R1R1	-0.17	0.37	0.646
SR1 vs. R1R1	0.76	0.39	0.0516
SR1 - (SS + R1R1)/2 (additivity)	0.76	0.32	1e-16
(R1R1 - SS) / R1R1 (selection, s)	-0.25	0.29	0.751
(SR1 - SS) / (R1R1 - SS) (dominance, h)	-1.29	5.10	0.751
SR2 mean	6.80	0.24	-
R2R2 mean	8.16	0.36	-
SS vs. SR2	-5.38	0.36	0
SS vs. R2R2	-6.72	0.42	0
SR2 vs. R2R2	-1.34	0.45	0.003
SR2 - (SS + R2R2)/2 (additivity)	1.87	0.35	1e-16
(R2R2 - SS) / R2R2 (selection, s)	3.83	1.05	1e-16
(SR2 - SS) / (R2R2 - SS) (dominance, h)	0.78	0.06	1e-16
SR3 mean	8.84	0.32	-
R3R3 mean	10.81	0.49	-
SS vs. SR3	-7.41	0.36	0
SS vs. R3R3	-9.37	0.79	0
SR3 vs. R3R3	-1.96	0.80	0.0145
SR3 - (SS + R3R3)/2 (additivity)	2.59	0.48	1e-16
(R3R3 - SS) / R3R3 (selection, s)	5.64	1.45	1e-16
(SR3 - SS) / (R3R3 - SS) (dominance, h)	0.77	0.07	1e-16

909

Extendend Data Table 2

Effect estimates from logistic model analysis for viability

Parameter	Viability	Std.Error	Lower.CI	Upper.CI	P.value
SS mean	0.89	0.01	-	-	-
SR1 mean	0.86	0.02	-	-	-
R1R1 mean	0.76	0.02	-	-	-
SS vs. SR1	1.42	0.27	-	-	0.0702
SS vs. R1R1	2.61	0.47	-	-	<.0001
SR1 vs. R1R1	1.84	0.30	-	-	4e-04
SR1 - (SS + R1R1)/2 (additivity)	0.03	0.02	-0.02	0.07	0.214
(R1R1 - SS) / R1R1 (selection, s)	-0.15	0.03	-0.2	-0.09	0.001
(SR1 - SS) / (R1R1 - SS) (dominance, h)	0.29	0.20	-0.15	0.64	0.214
SR2 mean	0.87	0.02	-	-	-
R2R2 mean	0.74	0.02	-	-	-
SS vs. SR2	1.28	0.25	-	-	0.205
SS vs. R2R2	2.96	0.53	-	-	<.0001
SR2 vs. R2R2	2.31	0.39	-	-	<.0001
SR2 - (SS + R2R2)/2 (additivity)	0.05	0.02	0.01	0.1	0.027
(R2R2 - SS) / R2R2 (selection, s)	-0.17	0.05	-0.28	-0.09	0.001
(SR2 - SS) / (R2R2 - SS) (dominance, h)	0.17	0.15	-0.15	0.45	0.027
SR3 mean	0.86	0.02	-	-	-
R3R3 mean	0.78	0.02	-	-	-
SS vs. SR3	1.42	0.27	-	-	0.0702
SS vs. R3R3	2.43	0.44	-	-	<.0001
SR3 vs. R3R3	1.72	0.29	-	-	0.0018
SR3 - (SS + R3R3)/2 (additivity)	0.02	0.02	-0.02	0.06	0.286
(R3R3 - SS) / R3R3 (selection, s)	-0.13	0.02	-0.18	-0.08	0.001
(SR3 - SS) / (R3R3 - SS) (dominance, h)	0.32	0.19	-0.15	0.67	0.286

910

Extendend Data Table 3

Effect estimates from linear model analysis for fecundity

Parameter	Fecundity	Std.Error	Lower.CI	Upper.CI	P.value
SS mean	200.22	11.99	-	-	-
SR1 mean	165.33	14.01	-	-	-
R1R1 mean	136.50	14.86	-	-	-
SS vs. SR1	34.89	19.81	-	-	0.14
SS vs. R1R1	63.72	20.42	-	-	0.01
SR1 vs. R1R1	28.83	20.42	-	-	0.17
SR1 - (SS + R1R1)/2 (additivity)	-3.03	17.26	-36.62	31.59	0.879
(R1R1 - SS) / R1R1 (selection, s)	-0.32	0.09	-0.48	-0.12	0.003
(SR1 - SS) / (R1R1 - SS) (dominance, h)	0.55	0.40	-0.07	1.32	0.881
SR2 mean	187.60	13.64	-	-	-
R2R2 mean	167.78	14.37	-	-	-
SS vs. SR2	12.62	19.81	-	-	0.53
SS vs. R2R2	32.44	20.33	-	-	0.37
SR2 vs. R2R2	19.82	19.81	-	-	0.49
SR2 - (SS + R2R2)/2 (additivity)	3.60	18.42	-33.15	43.16	0.834
(R2R2 - SS) / R2R2 (selection, s)	-0.16	0.09	-0.33	0.03	0.093
(SR2 - SS) / (R2R2 - SS) (dominance, h)	0.39	4.09	-2.3	3.23	0.842
SR3 mean	202.00	12.71	-	-	-
R3R3 mean	106.44	11.99	-	-	-
SS vs. SR3	-1.78	17.47	-	-	0.92
SS vs. R3R3	93.78	16.95	-	-	<.0001
SR3 vs. R3R3	95.56	17.47	-	-	<.0001
SR3 - (SS + R3R3)/2 (additivity)	48.67	12.84	22.41	73.56	1e-16
(R3R3 - SS) / R3R3 (selection, s)	-0.47	0.07	-0.59	-0.31	0.001
(SR3 - SS) / (R3R3 - SS) (dominance, h)	-0.02	0.19	-0.48	0.29	0.001

911

Extendend Data Table 4

Extended Data Table 4.1 Effect of time on malathion resistance (LD50) in treated cages

	During treatment				*After treatment*			
Predictors	**Estimates**	**std. Error**	**Statistic**	**p**	**Estimates**	**std. Error**	**Statistic**	**p**
Intercept	-3.02 ***	0.46	-6.58	**<0.001**	15.56 ***	1.09	14.29	**<0.001**
Time	2.48 ***	0.10	24.26	**<0.001**	-0.57 ***	0.14	-3.96	**0.001**
Random Effects								
σ^2	0.91				0.98			
τ_{00}	$0.00_{Treatment_Cage}$				$0.24_{Treatment_Cage}$			
ICC					0.20			
N	$10_{Treatment_Cage}$				$10_{Treatment_Cage}$			
Observations	40				30			
Marginal R^2 / Conditional R^2	0.938 / NA				0.302 / 0.441			
AIC	122.513				101.066			

** p<0.05 ** p<0.01 *** p<0.001*

Extended Data Table 4.2 Effect of time on malathion resistance (LD50) in untreated cages

	Beginning of treatment to end of experiment			
Predictors	**Estimates**	**std. Error**	**Statistic**	**p**
Intercept	2.27 ***	0.15	14.91	**<0.001**
Time	0.03	0.02	1.07	0.288
Random Effects				
σ^2	0.16			
$\tau_{00\ Treatment_Cage}$	0.03			
ICC	0.15			
$N_{Treatment_Cage}$	10			
Observations	59			
Marginal R^2 / Conditional R^2	0.017 / 0.166			
AIC	83.651			

** p<0.05 ** p<0.01 *** p<0.001*

912

Extendend Data Table 5

Extended Data Table 5.1 Effect of time on S (IGFG) frequency in treated cages

	During treatment				*After treatment*			
Predictors	**Estimates**	**std. Error**	**Statistic**	**p**	**Estimates**	**std. Error**	**Statistic**	**p**
Intercept	0.88 ***	0.02	49.15	**<0.001**	0.04	0.05	0.74	0.468
Time	-0.13 ***	0.00	-30.81	**<0.001**	0.02 *	0.01	2.64	**0.014**
Random Effects								
σ^2	0.00				0.00			
τ_{00}	0.00_{cage}				0.00_{cage}			
N	10_{cage}				10_{cage}			
Observations	50				30			
Marginal R^2 / Conditional R^2	0.951 / NA				0.194 / NA			
AIC	-148.876				-97.774			

** p<0.05 ** p<0.01 *** p<0.001*

Extended Data Table 5.2 Effect of time on R1 (VGFG) frequency in treated cages

	During treatment				*After treatment*			
Predictors	**Estimates**	**std. Error**	**Statistic**	**p**	**Estimates**	**std. Error**	**Statistic**	**p**
Intercept	0.08 ***	0.00	16.13	**<0.001**	0.04 **	0.01	3.09	**0.005**
Time	-0.00 ***	0.00	-4.05	**<0.001**	0.00	0.00	0.46	0.651
Random Effects								
σ^2	0.00				0.00			
τ_{00}	0.00_{cage}				0.00_{cage}			
ICC					0.25			
N	10_{cage}				10_{cage}			
Observations	50				30			
Marginal R^2 / Conditional R^2	0.251 / NA				0.005 / 0.250			
AIC	-276.043				-162.492			

** p<0.05 ** p<0.01 *** p<0.001*

Extended Data Table 5.3 Effect of time on R2 (VGFA) frequency in treated cages

	During treatment				*After treatment*			
Predictors	**Estimates**	**std. Error**	**Statistic**	**p**	**Estimates**	**std. Error**	**Statistic**	**p**
Intercept	0.01	0.01	0.93	0.356	0.14 **	0.04	3.39	**0.002**
Time	0.04 ***	0.00	13.93	**<0.001**	0.02 **	0.01	3.03	**0.006**
Random Effects								
σ^2	0.00				0.00			
τ_{00}	0.00_{cage}				0.00_{cage}			
N	10_{cage}				10_{cage}			
Observations	50				30			
Marginal R^2 / Conditional R^2	0.798 / NA				0.240 / NA			
AIC	-178.169				-107.043			

** p<0.05 ** p<0.01 *** p<0.001*

Extended Data Table 5.4 Effect of time on R3 (VAYG) frequency in treated cages

	During treatment				*After treatment*			
Predictors	**Estimates**	**std. Error**	**Statistic**	**p**	**Estimates**	**std. Error**	**Statistic**	**p**
Intercept	0.03	0.01	1.88	0.067	0.78 ***	0.05	15.18	**<0.001**
Time	0.09 ***	0.00	27.59	**<0.001**	-0.04 ***	0.01	-5.18	**<0.001**
Random Effects								
σ^2	0.00				0.00			
τ_{00}	0.00_{cage}				0.00_{cage}			
ICC	0.04							
N	10_{cage}				10_{cage}			
Observations	50				30			
Marginal R^2 / Conditional R^2	0.937 / 0.940				0.481 / NA			
AIC	-170.172				-96.128			

** p<0.05 ** p<0.01 *** p<0.001*

913

Extendend Data Table 6

Extended Data Table 6.1 Effect of time on S (IGFG) haplotype frequency in untreated cages

	Beginning of treatment to end of experiment			
Predictors	**Estimates**	**std. Error**	**Statistic**	**p**
Intercept	0.63 ***	0.02	39.49	**<0.001**
Time	0.00	0.00	0.21	0.838
Random Effects				
σ^2		0.00		
$\tau_{00\ cage}$		0.00		
ICC		0.03		
N_{cage}		10		
Observations		69		
Marginal R^2 / Conditional R^2		0.001 / 0.032		
AIC		-196.762		

** p<0.05 ** p<0.01 *** p<0.001*

Extended Data Table 6.2 Effect of time on R1 (VGFG) haplotype frequency in untreated cages

	Beginning of treatment to end of experiment			
Predictors	**Estimates**	**std. Error**	**Statistic**	**p**
Intercept	0.06 ***	0.00	14.68	**<0.001**
Time	0.00	0.00	1.91	0.061
Random Effects				
σ^2		0.00		
$\tau_{00\ cage}$		0.00		
N_{cage}		10		
Observations		69		
Marginal R^2 / Conditional R^2		0.051 / NA		
AIC		-370.061		

** p<0.05 ** p<0.01 *** p<0.001*

Extended Data Table 6.3 Effect of time on R2 (VGFA) haplotype frequency in untreated cages

	Beginning of treatment to end of experiment			
Predictors	**Estimates**	**std. Error**	**Statistic**	**p**
Intercept	0.07 ***	0.01	9.08	**<0.001**
Time	-0.00	0.00	-0.02	0.985
Random Effects				
σ^2		0.00		
$\tau_{00\ cage}$		0.00		
ICC		0.02		
N_{cage}		10		
Observations		69		
Marginal R^2 / Conditional R^2		0.000 / 0.024		
AIC		-285.686		

** p<0.05 ** p<0.01 *** p<0.001*

Extended Data Table 6.4 Effect of time on R3 (VAYG) haplotype frequency in untreated cages

	Beginning of treatment to end of experiment			
Predictors	**Estimates**	**std. Error**	**Statistic**	**p**
Intercept	0.24 ***	0.01	17.99	**<0.001**
Time	-0.00	0.00	-0.86	0.392
Random Effects				
σ^2		0.00		
$\tau_{00\ cage}$		0.00		
ICC		0.05		
N_{cage}		10		
Observations		69		
Marginal R^2 / Conditional R^2		0.010 / 0.064		
AIC		-222.940		

** p<0.05 ** p<0.01 *** p<0.001*

914